THE PARAMETERIZATION SCHEME OF THE ECMWF GRIDPOINT MODEL

BY

MICHAEL TIEDTKE

EUROPEAN CENTRE FOR MEDIUM RANGE WEATHER FORECASTS

1. Introduction

In the past the ECMWF has made considerable efforts to design a model for operational medium range weather forecasts. Up to now final decisions have only been made for the adiabatic part of the model. The first operational model will be a gridpoint model, which will have about 15 levels and a grid length of about 1.5^{o} in the horizontal. The spatial differencing scheme will be a second order scheme. For an adiabatic flow it will conserve global means of mass, moisture, total energy and for a barotropic flow it will conserve potential vorticity and enstrophy.

The non-adiabatic part of the model has not yet been finally decided. This is mainly because we do not know at present how accurately the various non-adiabatic processes must be simulated in a model for medium range weather forecasts.

In recent years meteorologists have concentrated mainly on short range weather prediction. According to Miyakoda (1975) and others, short range weather prediction may be most effectively improved by reducing the grid resolution and the initial state rather than by improving the parameterisation of subsynoptic processes. This may be so, because the short range changes of the large scale flow are mainly determined by the large scale flow itself and are less affected by the feed-back with the subsynoptic flow.

However, the interaction of different scales becomes more important for longer term developments, not at least because the external forcing occurs in the subsynoptic scale. Unfortunately, qualitatively little is known about the response time of subsynoptic scale motions and synoptic scale motions, which may even differ greatly for different subsynoptic processes. We do not know, therefore, whether the diurnal variation of radiation, clouds or the air-sea interaction must be considered in the model. Besides that, it is not proved whether the scale interaction can be simulated by the presently used parameterisation schemes to a sufficient accuracy for medium range weather prediction purposes.

Because of these uncertainties we have decided to adopt several different schemes and to test them in forecast experiments. In one place we also use the whole physics scheme of the GFDL general circulation model. It serves mainly as a reference scheme to examine the more sophisticated schemes. All of the schemes have been tested by some special experiments, but up to now not all of them have been tested in our three-dimensional forecast model. Thus, when we test them in global forecasts, we shall probably make slight changes. The schemes described below may therefore differ from those finally used.

2. The model equations

The equations of the model may be written in symbolic form as follows (for λ, φ, σ coordinates):

Equation of momentum

$$\frac{\partial}{\partial t}(p_* v) = A_v - g\frac{\partial}{\partial \sigma}\left(\tau^T + \tau^C\right) + F_m^T + F_m^C \qquad (1)$$

where v is the horizontal wind, p_* the surface pressure, A_v includes the advection term, the pressure gradient term and the Coriolis term; τ^T, τ^C are the downward fluxes of momentum due to turbulent and convective motions, respectively; F_m^T and F_m^C are the frictional forces due to turbulent and convective motions in the horizontal direction, respectively.

Thermodynamic equation

$$\frac{\partial}{\partial t}(p_* T) = A_T + p_*\frac{L_1}{c_p}(C-E) + p_* Q + \frac{g}{c_p}\frac{\partial}{\partial \sigma}\left(H^T + H^C\right) + F_T^T + F_T^C \qquad (2)$$

where T is temperature, A_T includes all adiabatic terms, C and E are the rates of condensation and evaporation respectively; Q is the radiative heating / cooling; H^T and H^C are the upward fluxes of sensible heat due to turbulent and convective motions, respectively; F_T^T and F_T^C represent heating / cooling by turbulent and convective motions in the horizontal directions, respectively; L_1 is the latent heat of condensation.

Equation of moisture

$$\frac{\partial}{\partial t}(p_* q) = A_q + p_*(E-C) + g\frac{\partial}{\partial \sigma}\left(R^T + R^C\right) + F_q^T + F_q^C \qquad (3)$$

q is the mixing ratio; A_q is the moisture advection; R^T and R^C are the vertical fluxes of moisture due to turbulent and convective motion respectively. F_q^T and F_q^C are the contributions of horizontal mixing due to turbulent and convective motions.

By (3) the model does not include clouds. Thus, the liquid water created by supersaturation instantaneously falls out.

As an alternative, we explicitly carry non-convective clouds in the model by means of predicting the total moisture (water vapour + cloud water):

$$\frac{\partial}{\partial t}\left(p_*(q+q_c)\right) = A_{q+q_c} + \frac{\partial}{\partial \sigma}\left(R^T + R^C\right) + F_{q+q_c}^T + F_{q+q_c}^C + p_* C_w \qquad (3a)$$

q_c is the mixing ratio of cloud water, A_{q+q_c} is the advection of total moisture, C_w includes the conversion rate between cloud water and rain water (transformation of cloud droplets into rain droplets) and the evaporation of rain in non-saturated air. Both kinds of processes are parameterized according to the simple cloud model proposed by Kessler (1969).

The precipitation rate at level σ is then :

$$P_\sigma = -\frac{p_*}{g}\int_0^\sigma C_w \, d\sigma \qquad (4)$$

3. Parameterization schemes

In equations (1) to (3) the parameterization of the different processes is not specified. However, we have formally distinguished two scales of sub-grid scale processes, namely those of the convective motions being more or less organised and those of the turbulent motions being truely random. This distinction seems necessary in principle, as we observe two pronounced scales of subsynoptic processes which are separated by a well known gap. However, it is worth noting that the model equations (1) to (3) do not result from a precisely defined avering procedure, but from putting together the effects of the different sub-grid processes, which are all parameterized by empirical assumptions.

A survey of the parameterization schemes which we shall use in our global model is listed in Table 1.

All of these schemes are more or less standard schemes and have been tested in various models in the past. The parameterization schemes shown in the second column are those of the GFDL general circulation model, in the third column we show the more sophisticated schemes.

TABLE 1
PARAMETERIZATION SCHEMES

PROCESS	GFDL MODEL	ECMWF MODEL
Convective motion		
Dry convection	Dry convective adjustment	Vertical diffusion type
Cumulus convection	Moist adiab. adjustment	Kuo-type scheme or diffusion-type
Turbulent motion		
Horizontal diff. Surface fluxes	Non-linear, 2nd order $F_x \sim C_d \mathbb{V}_h / (X_h - X_o)$	Non-linear, 2nd order $F_x \sim C_d \mathbb{V}_h / (X_h - X_o)$
	C_d = constant	$C_d = C_d(\frac{\partial \theta}{\partial Z}, \frac{h}{Z_o})$
Fluxes for Z>h	K-approach for momentum and moisture	K-approach for sensible heat, momentum and moisture
	$K = K(\ell)$	$K = K(\frac{\partial \theta}{\partial Z}, \ell)$
Surface values		
T_s Ocean	specified (climatological)	Specified (climatolog.)
T_s Land	diagnostically determined by surface heat balance equation	Predicted
Soil moisture	Predicted	Predicted
Snow	Predicted	Predicted
Radiation	Using climatologically specified cloud cover	Cloud cover from model-humidity or from predicted Clouds
Diurnal cycle	———	yes/no
Clouds	———	Cloud liquid water content predicted (cloud physics after Kessler (1969))

3.1 Horizontal diffusion by turbulent motion

The scheme used at present in the ECMWF model is the non-linear diffusion scheme proposed by Smagorinsky (1963). Following the notation of Miyakoda et al (1971), we use in our experiments for k_o the values $k_o = 0.1$ and $k_o = 0.2$.

3.2 Vertical fluxes of momentum, sensible heat and moisture due to turbulent motion

In the past a number of schemes have been proposed by several authors to parameterize the turbulent fluxes in the planetary boundary layer. Among those schemes the scheme which considers explicitly the surface layer (constant stress layer) and which uses the mixing length theory above the surface layer, seems most suitable for our model, as the boundary layer will be adequately resolved in the ECMWF forecast model (by at least 4 layers).

This scheme is rather simple and works reasonably well, even for its simple version as used in the GFDL-model. In contrast to other schemes, its application is not limited to the boundary layer but can be applied throughout the whole atmosphere.

The calculation of the turbulent fluxes is different for the surface layer and for the layers above.

Surface flux calculation

(a) GFDL-model

In the GFDL-model the turbulent fluxes at the surface are simply calculated by (Smagorinsky (1963)) :

$$\begin{aligned} \tau_o^{\top} &= \rho_h \, C_d \, |v_h| \, v_h \\ H_o^{\top} &= c_p \rho_h \, C_d \, |v_h| \, \left(T_o - T_h / \sigma_h^{R/c_p} \right) \\ R_o^{\top} &= D_w \rho_h \, C_d \, |v_h| \, \left(q_s(T_o) - q_h \right) \end{aligned} \qquad (5)$$

where C_d is the drag coefficient; c_p is the heat capacity; the subscrips 0 and h refer to the surface and to the top of the surface layer, which is assumed to be the height of the lowest prognostic level in the model; $q_s\ (T_o)$ is the saturation mixing ratio for water vapour at temperature T_o. The calculation of the evaporation follows a proposal of Budyko (1956), who suggests that the evaporation is the potential evaporation times the ground-wetness D_w (for further details on the evaporation calculation see GARP Publications Series No. 14, June 1974, p. 21).

The expressions for the surface fluxes are developed for a neutral stratification and therefore do not take the influence of stability into account. Also, the drag coefficient is assumed constant, having the same value $C_d = 2.0\ 10^{-3}$ over land and ocean.

(b) ECMWF-model

For medium range weather forecasts the flux calculations by (5) may be too crude. A refined scheme was therefore designed, based on the Monin-Obukhov similarity theory, for our model (Louis (1977)). The expressions for the fluxes have the form

$$(F_x)_o = f\left(\frac{h}{z_o}, |v_h|, \theta_h - \theta_o\right)(x_h - x_o).$$

Thus, the effects of stability and surface roughness z_o are considered. The expressions differ for a stable and an unstable stratified surface layer. We use the following expressions for an unstable stratified surface layer :

$$\tau_o^T = \rho_h a \left[|v_h| - \frac{b x}{|v_h| + a b c_m \left(\frac{h}{z_o}\right)^{1/2} x^{1/2}}\right] v_h$$

$$H_o^T = \rho_h \frac{a}{d}\left[|v_h| - \frac{b x}{|v_h| + a b c_H \left(\frac{h}{z_o}\right)^{1/2} x^{1/2}}\right]\left(T_o - T_h/\sigma_h^{R/c_p}\right) \qquad (6a)$$

with $$x = \frac{g h (\theta_h - \theta_o)}{\theta_h}$$

For a stable stratified surface layer we use :

$$\tau_o^T = \rho_h a \left(\frac{1}{1 + \frac{b \cdot x}{2|v_h|^2}}\right)^2 |v_h| v_h$$

$$H_o^T = \rho_h \frac{a}{d}\left(\frac{1}{1 + \frac{b x}{2|v_h|^2}}\right)^2 |v_h|\left(T_o - T_h/\sigma_h^{R/c_p}\right) \qquad (6b)$$

The values of the parameters are:

b=9.4, d=0.74, c_m=7.4, c_H=5.3

$a = k^2/\left(\ln \frac{h}{z_o}\right)^2$ with k=0.35 (von Karman's constant).

The moisture flux is calculated using the same values as for the sensible heat flux.

Calculation of the fluxes above the surface layer

Above the surface layer we calculate the fluxes by means of the mixing length theory. Besides the GFDL-scheme, we use an improved scheme which again considers the effect of stability on the turbulent fluxes. For the improved scheme the fluxes are calculated for the whole atmosphere, whereas in the GFDL-model they are calculated only for the layer below about 700 mb. The fluxes are calculated for momentum, moisture and also for sensible heat in contrast to the GFDL-scheme, where the turbulent transfer of heat is neglected.

(a) GFDL-scheme

The fluxes of momentum and moisture are calculated on the basis of the mixing length theory for neutral stratification.

The vertical transfer of heat is ignored, assuming that the transfer for unstable stratification is sufficiently well described by the dry convection and that it is zero for stable conditions:

$$\begin{aligned} \tau^T &= \rho K \frac{\partial v}{\partial z} \\ R^T &= -\rho K \frac{\partial q}{\partial z} \\ H^T &= 0 \end{aligned} \qquad (7)$$

where the diffusion coefficient depends on wind shear and on the mixing length

$$K = \ell^2 \left| \frac{\partial v}{\partial z} \right| \qquad (8).$$

The mixing length ℓ depends on height as

$$\begin{aligned} \ell &= kz && \text{for } z \leq h \\ \ell &= kh \frac{H - z}{H - h} && \text{for } h < z \leq H \\ \ell &= 0 && \text{for } z > H \end{aligned}$$

with k=0.35, h=75m, H=2.500m.

(b) ECMWF-scheme

As for the surface layer, the thermal stratification is taken into account. The diffusion coefficient depends now on wind shear and on stability as

$$K = \ell^2 f\left(\left| \frac{\partial v}{\partial z} \right|, \frac{\partial \theta}{\partial z} \right)$$

The fluxes are calculated similarly to the surface layer for reasons of continuity. We have therefore different expressions for the diffusion coefficients for stable and unstable conditions. For unstable conditions the diffusion coefficient is :

$$K = \ell^2 \left(\left| \frac{\Delta v}{\Delta z} \right| - \frac{b \frac{g}{\theta} \frac{\Delta \theta}{\Delta z}}{\left| \frac{\Delta v}{\Delta z} \right| + c_m \left(\frac{\ell}{\Delta z} \right)^2 b \left(\left(\frac{z_{k+1}}{z_k} \right)^{1/3} - 1 \right)^{3/2} \left(\frac{g}{\theta} \left| \frac{\Delta \theta}{\Delta z} \right| \right)^{1/2}} \right) \qquad (9a)$$

and for stable conditions we use

$$K = \ell^2 \left| \frac{\Delta v}{\Delta z} \right| \Big/ \left(1 + \frac{\frac{b}{2} \frac{\Delta \theta}{\Delta z} g}{\theta \left(\frac{\Delta v}{\Delta z} \right)^2} \right)^2 \qquad (9b)$$

where the differences $\Delta v, \Delta \theta, \Delta z$ are evaluated from the corresponding values of the two next levels k and k+1.

The mixing length ℓ depends on height.

The calculations are made throughout the atmosphere for momentum, sensible heat and moisture.

For sensible heat and moisture calculations, c_m in (9) must be replaced by c_H, and K in (9a) must be divided by 0.74.

3.3 Specification of surface values

To compute the heat fluxes and the moisture fluxes, temperature and ground wetness must be known at the surface. Again, the GFDL scheme served as a starting point. Since the surface processes are considered to be fairly complete in this scheme, we decided to use this scheme in our model. However, some refinements become necessary, as the diurnal variation of the solar radiation will be considered in the model.

In the GFDL-model the surface temperature is specified over the sea

$$T_o = (\text{Tsea})\big|_{\text{surface}}$$

Over land the surface temperature is determined such that a surface heat balance exists:

$$\sigma_B T_o^4 - (1-A) S_o - F_o + H_o^T + L_1 R_o^T + L_2 M = 0 \qquad (10)$$

where σ_B is the Stefan-Boltzmann constant, A the albedo, S_o the insulation, F_o the downward longwave radiation, M the snow-melt, L_1 the latent heat of condensation and L_2 the latent heat of the ice melting.

The heat balance equation (10) is successfully used in models which do not consider the diurnal variation of insulation. However, when the diurnal change of radiation is considered in the model, the heat conduction in the soil must be considered. The diagnostic relation (10) in the ECMWF model is therefore replaced by a prognostic equation for the surface temperature.

$$C_s \frac{\partial T_o}{\partial t} + \sigma_B T_o^4 - (1-A) S_o - F_o + H_o^T + L_1 R_o^T + L_2 M + B = 0 \qquad (11)$$

where C_s is the thermal capacity per unit lateral of the surface layer in the soil and B is the heat conduction to the sub-surface layer in the soil. B is parameterized by

$$B = \lambda \frac{T_o - T_B}{\Delta z}$$

where is the thermal conductivity and T_B is a fixed temperature in the soil (at $z = -\Delta z$).

The hydrology of the land surface is considered in the same way as proposed by Budyko (1956) and as is used in the GFDL-model (GARP Publications, Series No.14, June 1974, pp.20-23).

Soil water and snow amounts are predicted by taking into account the following processes : rainfall, evaporation, run-off, snow-melt and snow-fall.

3.4 Convection

(a) Dry convection

Subgrid scale fluxes due to dry convection are considered either by means of the dry adiabatic adjustment process, as is used in the GFDL-model, or by means of a vertical diffusion type.

The dry adjustment scheme works only on the temperature field; whereas the diffusion scheme may include also moisture and momentum fluxes. The diffusion type may be written as

$$H^c = \frac{\partial}{\partial \sigma}\left(\left(\frac{g\sigma}{RT}\right)^2 K \frac{T}{\Theta}\frac{\partial \Theta}{\partial \sigma}\right)$$

$$R^c = \frac{\partial}{\partial \sigma}\left(\left(\frac{g\sigma}{RT}\right)^2 K \frac{\partial q}{\partial \sigma}\right) \qquad (12)$$

where the diffusion coefficient K depends on stability $K=K\left(\frac{\partial \Theta}{\partial \sigma}\right)$ being zero for stable conditions.

(b) Moist convection

The parameterization of moist convection is one of the most serious problems since very little is known about the interaction of convection with the large-scale flow.

The two schemes used in our model are the moist convective adjustment scheme proposed by Manabe et al (1956) and being used in the GFDL-general circulation model, and the convection scheme proposed by Kuo (1974).

The Manabe-scheme is one of the simplest schemes and represents directly the gross stabilizing effects of convection on the environment by adjusting the temperature field and the moisture field towards a moist neutral state. The adjustment is made for a layer, which is

(1) saturated everywhere ($f \geq 100\%$) and
(2) which is moist-adiabatically unstable stratified

$$\frac{\partial T}{\partial \sigma} > \Gamma_e, \qquad \Gamma_e = \frac{RT}{c_p T}\,\frac{P + \frac{0.622}{RT} L_1 e_s}{P + \frac{0.622}{RT} L_1 \frac{\partial e_s}{\partial T}} \qquad (13)$$

(e_s = saturation water vapour pressure).

The new state after the adjustment has been made is then a moist adiabatic one

$$\frac{\partial T^N}{\partial \sigma} = \Gamma_e(T^N, q^N), \quad q^N = q_s(T^N) \tag{14}$$

where N denotes the new state. There are mainly two disadvantages of this scheme. The first one is the saturation criterion, which allows convection to occur only in saturated air whereas convection generally occurs in non-saturated environmental air. Secondly, this scheme involves sudden changes, as the adjustment takes place instantaneously and is done completely. This may lead to unacceptably large values of vertical motion in regions of convective adjustment.

The second scheme used is the scheme designed by Kuo (1965,1974) for parameterizing deep convection in tropical regions. It considers the effect of cumulus clouds on the large scale flow by using a realistic but simple model of cumulus clouds themselves. Cumulus clouds are assumed to be forced by mean low-level convergence but only exist in regions of conditionally unstable stratification.

Cloud basis, distribution of temperature and moisture within the cloud and the cloud top are determined thermodynamically, neglecting entrainment and detrainment. The production of cloud air is then assumed to be proportional to the net amount of moisture convergence into one grid point column plus surface evaporation.

The total accession of moisture per unit square is given by

$$I = \frac{1}{g}\int_0^1 A_q \, d\sigma + R_0^T \tag{15}$$

and the surplus of the total energy of the cloud air against the environment is given by

$$P = \frac{P_*}{g}\int_{\sigma_{TOP}}^{\sigma_{BOT}} \left[c_p(T_c - T_e) + L_1(q_c - q_e)\right] d\sigma \tag{16}$$

where the index c refers to cloud air and the index e refers to the environmental air. The fractional cloud area α being produced by the moisture supply then follows from

$$\alpha P = L_1 \cdot I \tag{17}$$

Thus, the environment is heated and moistened as

$$\Delta T = \alpha (T_c - \bar{T}_e)$$
$$\Delta q = \alpha (q_c - \bar{q}_e) \qquad (18)$$

Departing from the original scheme proposed by Kuo we do not only consider convective clouds originated by lifted surface air, but also clouds which are originated at upper levels where moisture convergence is observed. Besides that, we do not consider the moisture accession for the whole grid point column but only the accession which takes place in the layer between the lifting level and the top of the cloud.

The vertical transports of heat, moisture and momentum due to convective motions (H^c, R^c and $\bar{\tau}^c$) in eq. (1) to (3) which are generally ignored, may also be considered in this scheme (Kuo,1974, Anthes, 1977) by (taking moisture for example)

$$R^c \sim \overline{\omega' q'} = \frac{a}{1-a} (\omega_c - \omega_e)(q_c - q_e) \qquad (19)$$

where the mean updraft in the clouds ω_c and the fractional area a covered by clouds may be estimated using the cloud parameters, making assumptions on the mean lifetime τ of cumulus clouds.

Following Kuo (1974) the cloud cover may be determined from

$$a \cdot P = \tau \cdot I$$

and the vertical velocity ω_c by

$$\omega_c = - \frac{\theta_c - \theta_e}{\tau \frac{\partial \theta_e'}{\partial p}}$$

where $\frac{\partial \theta_e'}{\partial p}$ represents the mean vertical gradient of the equivalent potential temperature θ_e' in the unstable layer.

An alternate estimate of a and ω_c was proposed by Anthes (1977). The vertical velocity follows from the momentum equation for the vertical motion as

$$\frac{1}{2} \frac{dw_c^2}{dz} = g \frac{(T_v)_c - (T_v)_e}{(T_v)_e} - \mu w_c^2$$

where T_v is the virtual temperature and where μw_c^2 represents an entrainment process. We further assume that $\omega_c \simeq -g\varrho w_c$. The cloud cover a follows from the moisture equation assuming stationarity and neglecting horizontal moisture advection

$$\omega_c \frac{\partial q_c}{\partial p} = - C_c .$$

For the Kuo scheme the mean condensation equalizes the net heating dH

$$a L_1 C_c = dH$$

Thus a becomes:

$$a = \frac{dH}{-L_1 \int_{P_{TOP}}^{P_{BOT}} \omega_c \frac{\partial q_c}{\partial p} dp}$$

The horizontal diffusion due to convective motions is neglected ($F_m^c = 0$, $F_T^c = F_q^c = 0$).

3.5 Condensation processes

At present condensation processes are considered in numerical models in a rather crude way. Large-scale condensation occurs when moisture grid point values exceed the saturation value. The condensed water instantaneously falls out as precipitation. As cloud water is not considered explicitly in the model atmosphere, there is no reevaporation of clouds possible, which might reduce the total heating due to condensation processes and therefore might have significant effects on the flow, especially over longer periods. In order to see whether the inclusion of clouds has any significant effect on 10-day forecasts, we will perform tests with a scheme which considers explicitly cloud water. In this scheme we predict the total moisture (water vapour and cloud water) by (3a) rather than the water vapour only. The following processes are considered in the model

1. Condensation of water vapour q to cloud droplets (liquid water content q_c) -C.

2. Autoconversion of cloud droplets to rain drops - AC.

3. Collection of cloud droplets by rain drops - CC.

4. Evaporation of rain drops, when falling through non-saturated layers - E_r.

5. Evaporation of cloud droplets due to temperature increase - E_c.

Note that $E = E_c + E_r$ in (2), and $C_w = E_r - AC - CC$ in (3a) and (4).

Condensation of cloud water C and evaporation of cloud droplets E_c are determined diagnostically in the usual way by checking the forecasts of temperature and humidity for supersaturation and for saturation-deficit, respectively. The other cloud physical processes AC, CC and E_r are parameterized following a proposal of Kessler (1969).

The autoconversion is

$$AC = k_1 \left(q_c - \frac{a}{s} \right) \tag{19a}$$

where a is a critical value above which cloud droplets convert to raindrops.

The cloud collection is assumed to be

$$CC = k_2 q_c M^{7/8} \sqrt{\sigma} \tag{19b}$$

with $k_2 = 0$ for $q_c \leq 0$

$k_2 > 0$ for $q_c > 0$

$M(g/m^3)$ is the liquid water content of rain.

Evaporation of rain is parameterized as

$$E_r = k_3 (q - q_s) M^{13/20} \tag{19c}$$

with $k_3 = 0$ if $q \geq q_s$

$k_3 > 0$ if $q < q_s$

The liquid water content of rain M which is needed in (19), but which is not specified in the model explicitly, is assumed to be

$$M = \left(k_4 \sqrt{\sigma} P \right)^{8/9} \tag{19d}$$

where the rain intensity P is given by the model by (4).

4. Description of the experiments

As we have no clear understanding at present how 10-day forecasts are affected by the different processes included in the model, we decided to carry out so-called sensitivity tests, where numerical forecasts are performed with different parameterization schemes. The experiments recently performed are specified in Table 2. Except for the experiment N48, which was performed with the original GFDL-model, using the grid resolution N48 (48 grid points along a meridian between the Pole and the Equator), all experiments were performed using a coarse grid resolution N16/24 (24 grid points between the Pole and the Equator and 4 x 16 = 64 grid points along a latitude circle) Besides, the N48-forecast is made for a regular non staggered longitude-latitude grid using an energy conserving finite difference scheme, whereas all other runs are made for a staggered grid with a finite-difference scheme which also conserves potential enstrophy for an adiabatic barotropic flow. Experiment N04 uses the complete parameterization scheme of the GFDL-scheme except that a smaller diffusion coefficient k_o=0.1 is used. Experiment N06 is performed using the radiation scheme developed by Geleyn (1977) and in N09 the radiative heating/ cooling in the free atmosphere is neglected. The radiation calculation is, however, used to specify the surface temperature by (10). As the PBL-scheme developed by Louis (1977) is not yet included in our model, we made tests where the surface flux calculation in the GFDL-scheme was slightly changed. In experiment N10 the drag coefficient C_d was changed to C_d=0.0011 over sea and to C_d=0.0044 over land, whereas in all other experiments the drag coefficient was assumed constant C_d=0.002. In experiment N02 we use the Kuo-convection scheme and in all other experiments we use the moist convective adjustment scheme (Manabe-scheme). Besides, in N02 condensation takes place whenever the mixing ratio exceeds the saturation value whereas in all other runs condensation occurs if the relative humidity exceeds 80%. All forecasts started from the same initial state of 1.3.1965 (Fig. 1) .

5. Results from experiments with different grid resolution and with different surface flux calculations (N48,N04,N10).

In the first set of experiments we compare forecasts based on different grid resolutions (N48 and N16/24). For comparison we include also one experiment with different physics, i.e. changed surface flux calculations.
Figures 2 to 5 show the predicted height fields on day 2, day 4 and day 10 for the different forecast experiments, as well as the NMC analysis. The predicted fields show small differences up to 4 days, the forecast with the coarse grid being of the same quality as that with the smaller grid size. This is probably due to the fact that short range weather forecasts for, say, up to 3 or 4 days, are mainly determined by the linear properties of the model equations (wave propagation).

SPECIFICATION OF EXPERIMENTS

TABLE 2

Exp.	Convection	Radiation	PBL	Hor.Diffusion	Num. Scheme
N01	Manabe	GFDL	GFDL, C_d=0.002	k_o=0.2	ECMWF
N02	Kuo	GFDL	-dto.-	k_o=0.2	ECMWF
N03	Manabe	GFDL	-dto.-	no diffusion	ECMWF
N04	Manabe	GFDL	-dto.-	k_o=0.1	ECMWF
N06	Manabe	Geleyn	-dto.-	k_o=0.1	ECMWF
N09	Manabe	no rad. heat.	-dto.-	k_o=0.1	ECMWF
N10	Manabe	GFDL	C_d= 0.0011 / 0.0044	-dto.-	ECMWF
N11	No moist.	GFDL	C_d=0.002	No diff.	ECMWF
N48	Manabe	GFDL	C_d=0.002	k_o=0.25	GFDL

GRID RESOLUTION : N16/24 for Exp. N01 - N11

N48 for Exp. N48

According to Temperton's (1977) investigation of the normal modes of the finite difference scheme for our staggered grid compared with those for a non-staggered grid, the linear properties for the staggered grid are similar to those for a non-staggered grid of twice the grid resolution. Beyond day 4, however, the differences between the N48 forecast and the N16/24 - forecasts become significant and are rather large on day 10, the N10 and N04 forecasts showing a less intense zonal flow and much weaker eddies. On the other hand, the forecasts with the two different surface-flux calculations (N04 and N10) show comparably small differences even on day 10.

These results are confirmed by the diagnostic calculations made for the kinetic energy and for the available potential energy and, moreover, by the energy transformations between the zonal part and the eddies. Figures 6 - 10 show the energy diagnostics at different spectral ranges for the period between day 6 and day 10. The agreement between predicted and observed values is best for the experiment with the high resolution (N48), though the predicted values are generally smaller than observed values. The coarse grid experiments N04 and N10 show the deficiencies mentioned above - far too small amounts of kinetic and available potential energy at all spectral ranges, resulting in rates of energy transformations of too small a value. The differences between N04 (GFDL-radiation) and N10 (experiment with variable drag coefficient) are comparably small except for the energy transformation from the zonal available potential energy to that of wave numbers 4 to 9, which is much larger and more realistic in the forecast where the drag coefficient was assumed different over sea and over land.

5.1 Results from experiments with different horizontal diffusion (N01, N03, N04, N11)

In order to study the effect of horizontal diffusion of momentum moisture and sensible heat on a 10-day forecast, experiments were carried out using different values for the diffusion coefficients. In experiment N03 no horizontal diffusion was used, in experiment N01 a large value (k_o=0.2) was used and experiment N04 was made with a value of k_o=0.1 The value k_o=0.1 is close to the value k_o=0.13 suggested by Deardorff (1971). Experiment N11 was also performed without diffusion, but now for a dry model atmosphere (no condensation processes, no moist convective heating). From the results shown in Figures 11-16 we deduce : the forecasts without horizontal diffusion (N03 and N11) were numerically stable over the 10-day forecast period, but show, as expected, small scale eddies as can be seen from the predicted height fields (Figure 11) and from the diagnostics of energy. An extremely large amount of kinetic energy at wave numbers 10 - 20 was observed in the low latitude upper troposphere.

This was observed in both experiments N03 (which includes moisture processes) and N11 (which neglects these processes) as seen from Fig. 14. Up to now we do not know how these small scale eddies are generated; further investigations will be undertaken.These small scale eddies are successfully removed in the experiments with diffusion (N01,N04, etc.). However, at the same time, the large scale flow in mid- and high latitudes seems to be affected far too much, as is best seen by comparing the values for the generation of available potential energy at wave numbers 1 to 3 (Fig. 3) and at wave numbers 4 to 9 (Fig. 16). This strong influence of horizontal diffusion is probably partly due to the fact that a rather coarse grid resolution is used and becomes probably smaller with increased resolution.

5.2 Results from the experiments with different radiation calculations (N04,N06,N09)

The influence of radiation has been studied by carrying out experiments using different radiation schemes. Besides the GFDL radiation scheme (run N04), the radiation scheme developed by Geleyn (run N06) has been used. This scheme was designed in order to consider explicitly the feed back of clouds and radiation in the model. As clouds are not predicted at present, the cloud cover was assumed to depend on the relative humidity f at the level $\sigma = \sigma(p)$ as

$$c = \left(\frac{\max(f - \sigma, 0)}{1 - \sigma} \right)^2$$

For the purpose of comparison, an experiment was also performed where the net radiative heating was neglected. However, the radiative fluxes were used in order to specify the surface temperature over land by means of the surface heat balance equation (10).
The predicted height fields on day 10 showed only small differences at 500 mb for the two different radiation calculations (Fig. 17), but became larger at the surface (Fig.18), though the differences are smaller than compared with the experiment N10 with variable drag coefficients (Fig.18). These results are confirmed by the energy statistics which show also very small differences for the kinetic energy at all wave numbers. The only difference in the values of generation of available potential energy is found with wave numbers 1 to 3 and wave numbers 4 to 9.
In the experiment considering moisture-radiation interaction (N06), the observed maxima at about 40°N are reproduced better than those in the experiment N04 with the GFDL-radiation (Figures 21 - 22).
As expected, the forecast without radiative heating (N09) shows weaker eddies, although the decrease seems surprisingly low, which is probably due to the rather small diffusion coefficient (k_o=0.1) which was used. The most pronounced difference, however, is observed in the zonal mean temperatures, which on day 10 are about 5°C to 10°C higher than observed in the experiments with radiation.

5.3 Results from experiments with different moist convection schemes (N01 and N02)

The two moist convection schemes used are the moist adiabatic adjustment scheme (experiment N01) and the Kuo convection scheme (N02). As mentioned before, the critical mixing ratio above which condensation occurs in the model atmosphere is different for both runs, being smaller in the run with the moist adiabatic adjustment scheme ($f = 0.8$) than in the run with the Kuo-scheme ($f = 1.0$). Therefore, more moisture is allowed to be stored in the model atmosphere in the Kuo-run N02. This is confirmed by the values of precipitation and evaporation as shown in Table 3. For nearly the same amount of evaporation at the surface, a considerably smaller amount of precipitation was observed for run N02 compared with run N01. At the same time, however, the actual amount of precipitation due to convection was larger in the Kuo-run N02. The effect of the different treatment of convection on the height fields is small at 500 mb but pronounced at the surface (Fig.23), where stronger eddies in the forecast with the moist adiabatic adjustment scheme are observed. The evaluated energy statistics show small differences for the kinetic energy (not shown here) but significant differences for the available potential energy and the conversion rates. At mid latitudes, un N02 (Kuo-scheme) shows larger values of available potential energy for wave numbers 4 to 9 (Fig. 25) but smaller values for the higher wave numbers 10 to 20 (Fig. 26). The same is observed for the conversion rates.

T A B L E 3

GLOBAL MEANS OF LARGE SCALE PRECIPITATION P_L, PRECIPITATION DUE TO CONVECTION P_c AND EVAPORATION E FOR RUN N01 AND N02

	P_L	P_c	E
N01(Adjustm.)	16	14	32
N02(Kuo)	7	15	31

6. Concluding remarks

Numerical 10-day forecasts have been performed with different parameterization schemes (GFDL-scheme and ECMWF-scheme) and with two different grid resolutions (N16/24 and N48). The results show that for the chosen grid resolution N16/24, the 10-day forecasts are far more sensitive to the increase of the grid resolution than to the changes in the parameterization of subgrid scale processes. The change from one parameterization scheme to another yields significant changes, mainly in the generation of available potential energy and causes changes in the transformation from zonal to eddy available potential energy. The largest changes are observed when the coefficient for the horizontal diffusion of momentum, moisture and sensible heat are altered. The replacement of the moist adiabatic adjustment scheme by the convection scheme designed by Kuo(1965), the replacement of the GFDL-radiation-scheme by the scheme proposed by Geleyn (1977) and the modification of the surface flux calculation gave smaller changes.

The comparably weak sensitivity observed for the parameterization of subgrid scale processes is probably due to the fact that a rather coarse grid resolution has been used. The sensitivity will presumably be stronger for higher grid resolutions. Besides, the parameterization scheme has been altered only in some parts and the sensitivity will increase when the parameterization scheme will be completely replaced.

F I G U R E S

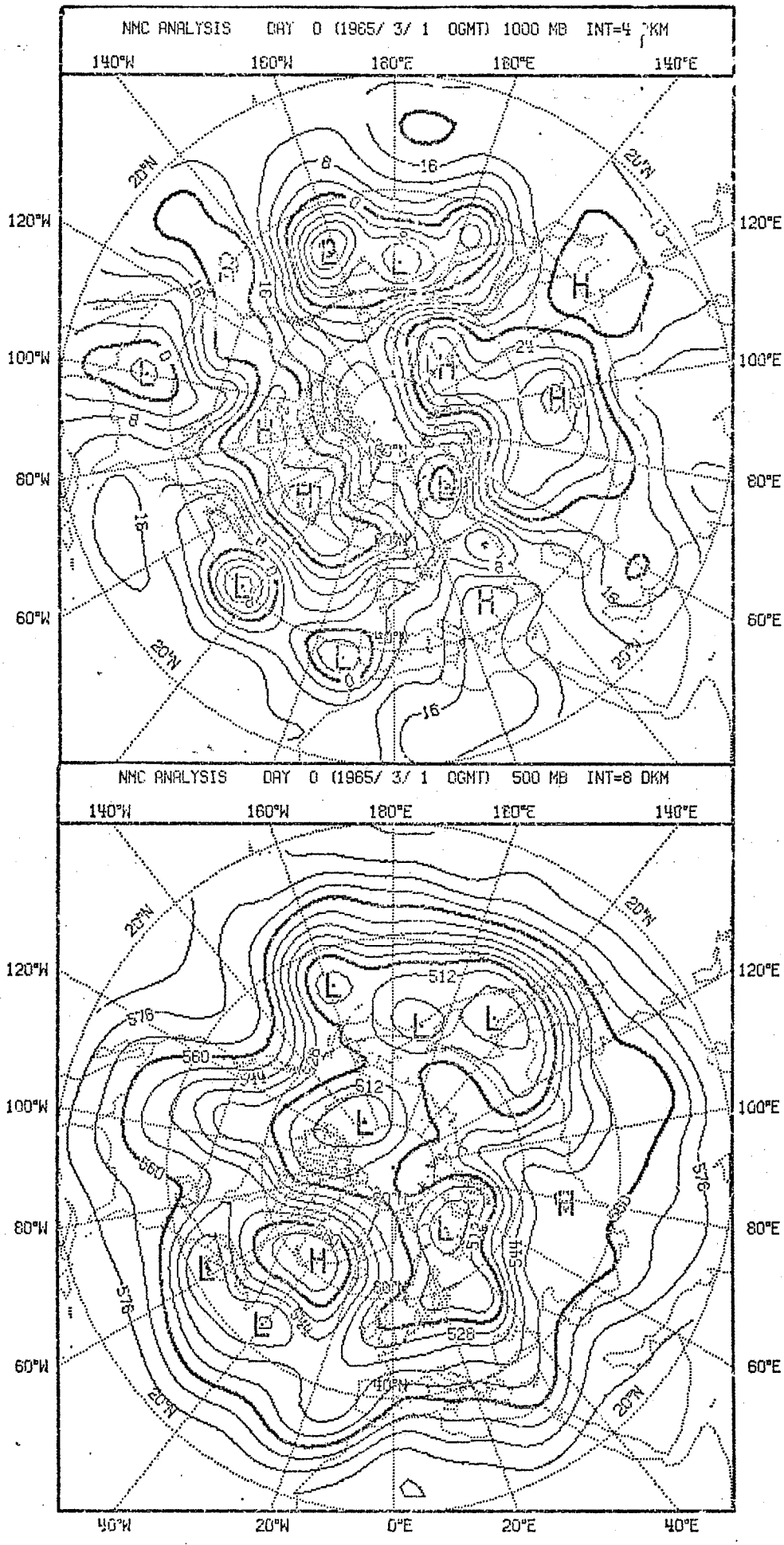

Figure 1 Initial height distribution at 500 mb and at 1000 mb (1.3.1965)

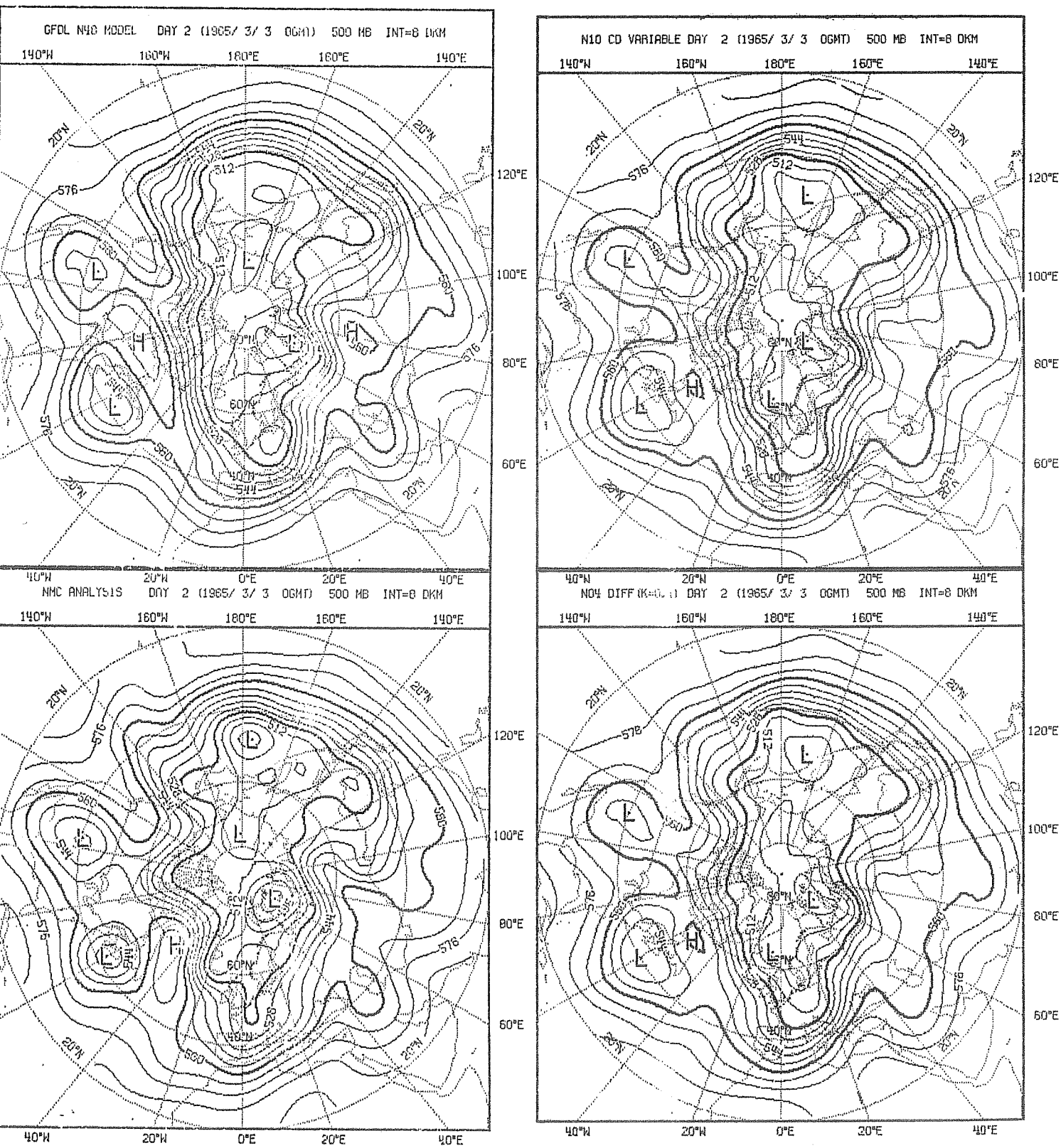

Figure 2 Height at 500 mb at day 2 (3.3.1965) for NMC-Analysis and Run N48, N10 and N04.

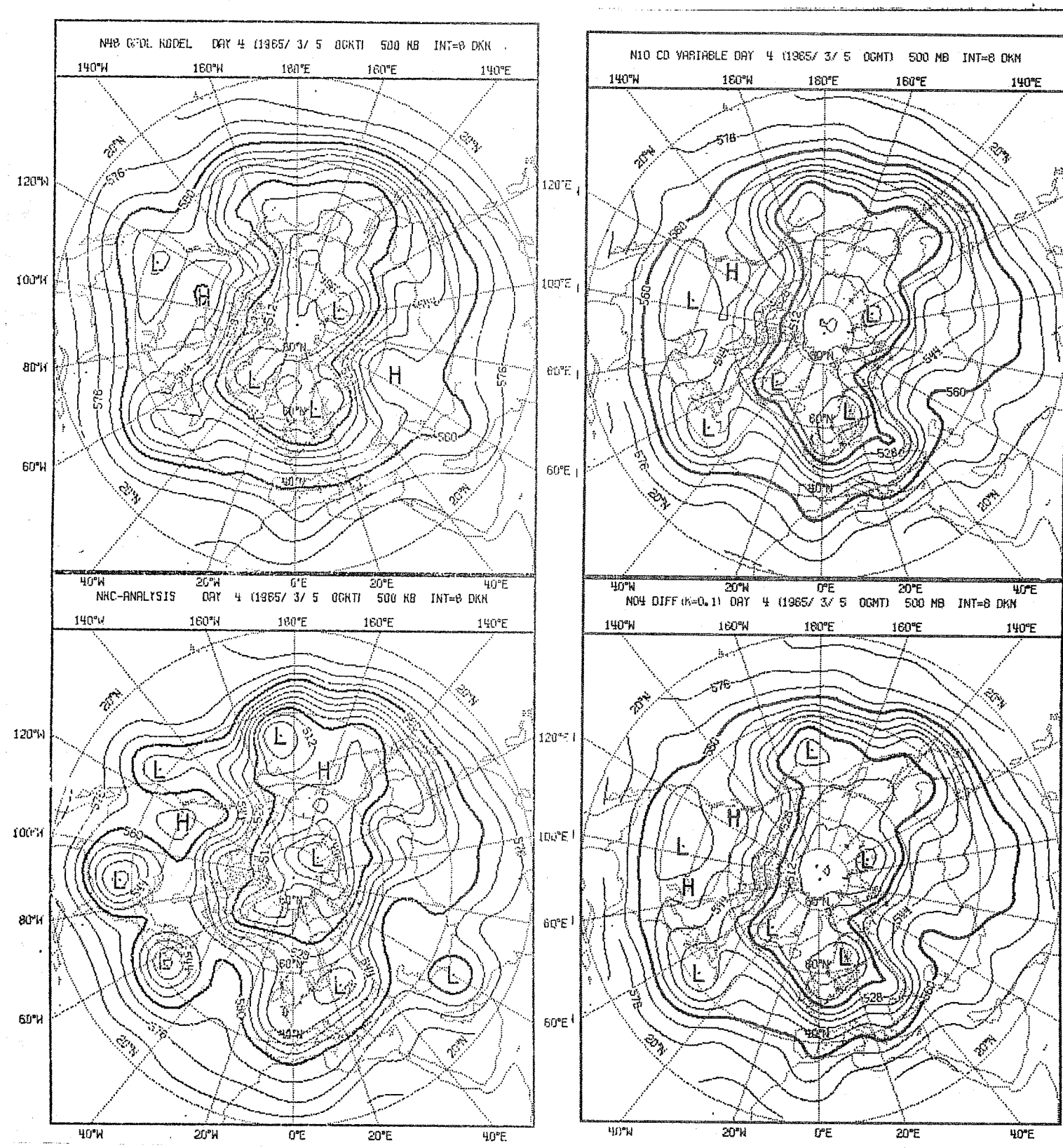

Figure 3 Height at 500 mb at day 4 (5.3.1965) for NMC-Analysis and Run N48, N10 and N04.

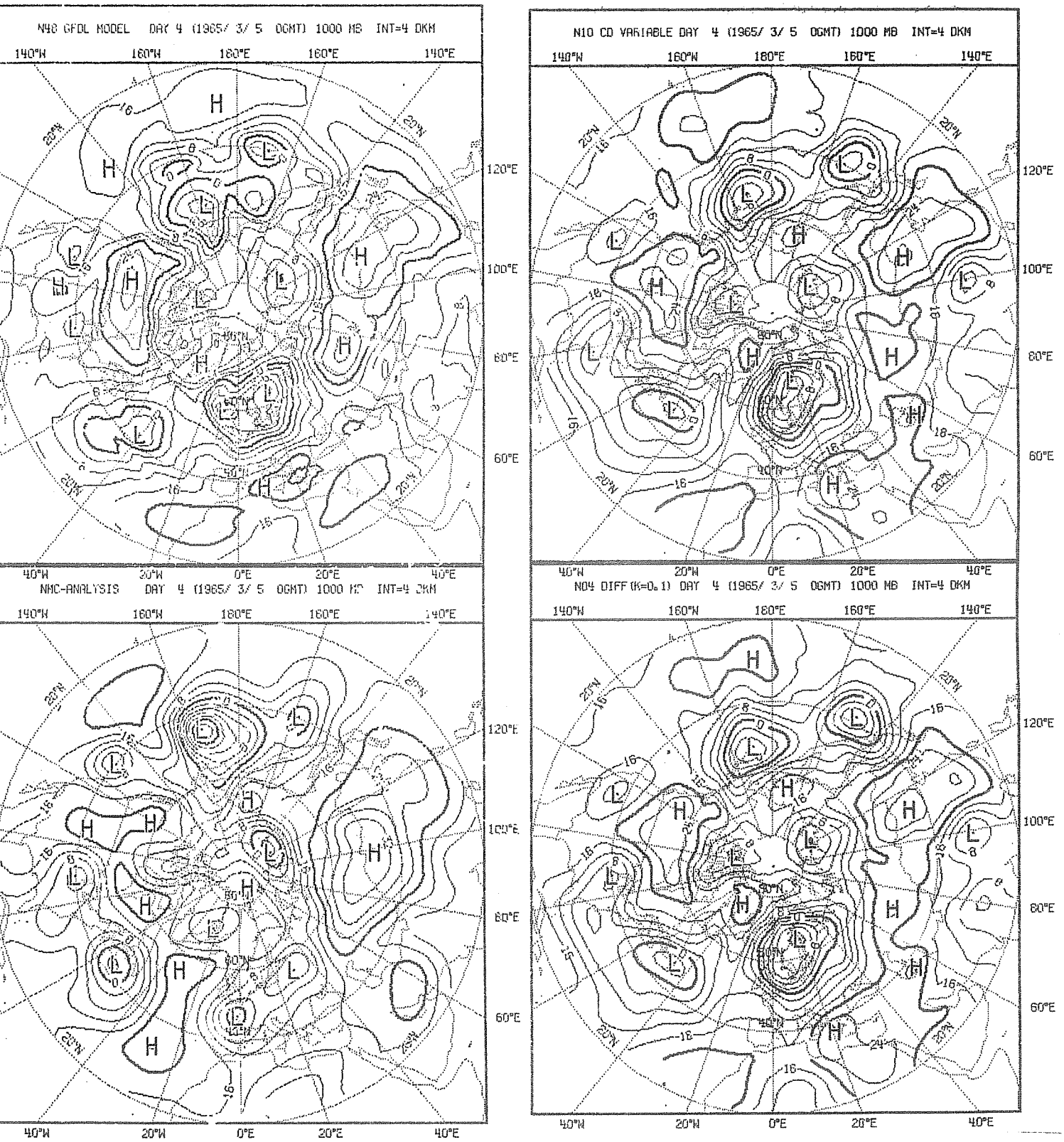

Figure 4 Height at 1000 mb at day 4 (5.3.1965) for NMC-Analysis and Run N48,N10 and N04.

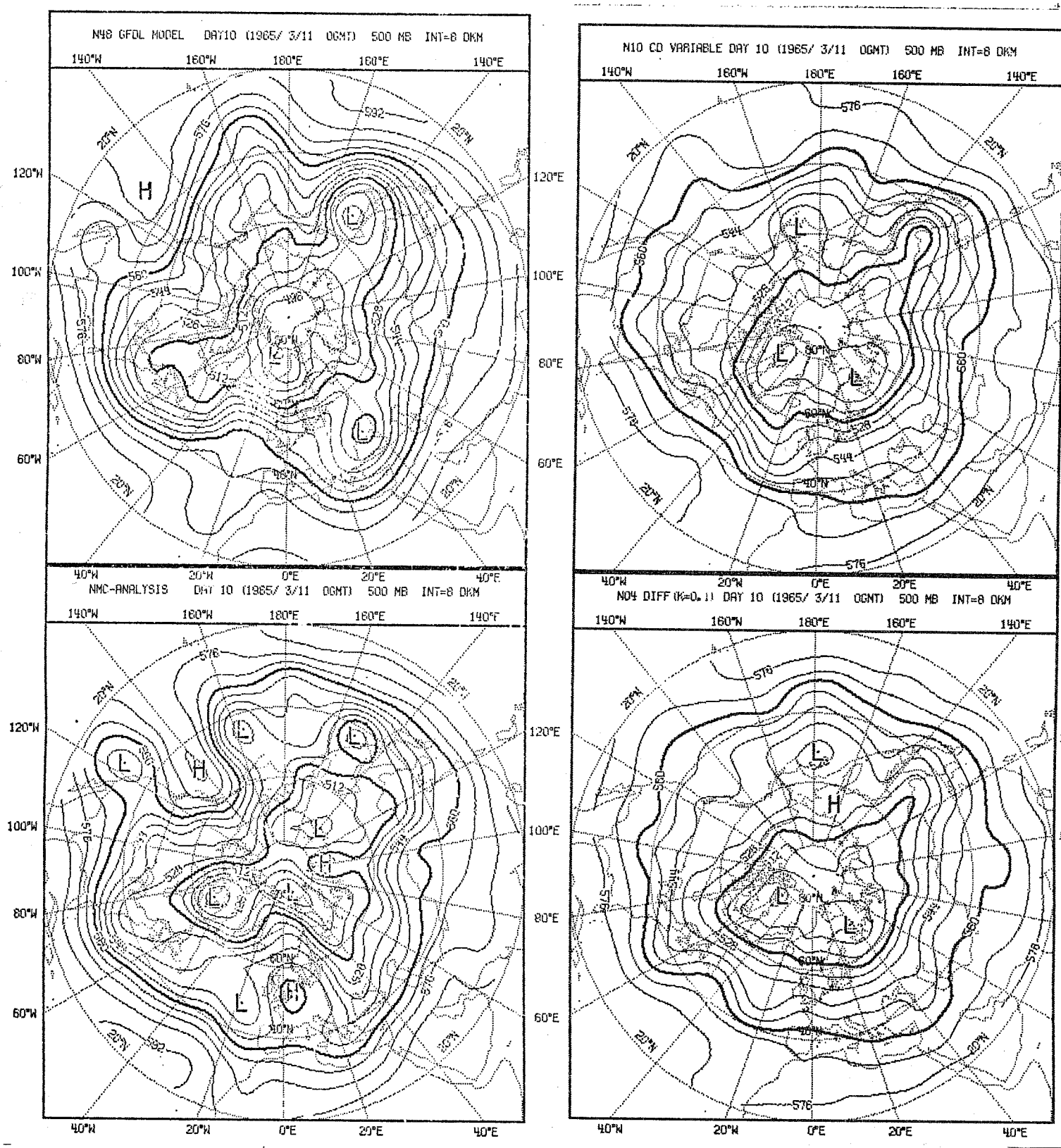

Figure 5 Height at 500 mb at day 10 (11.3.1965) for NMC-Analysis and Run N48, N10 and N04.

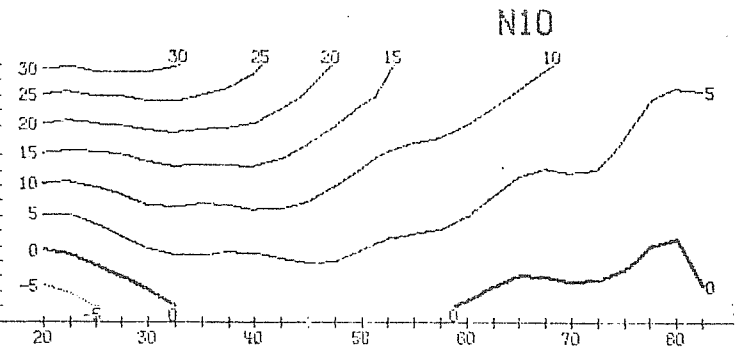
N10

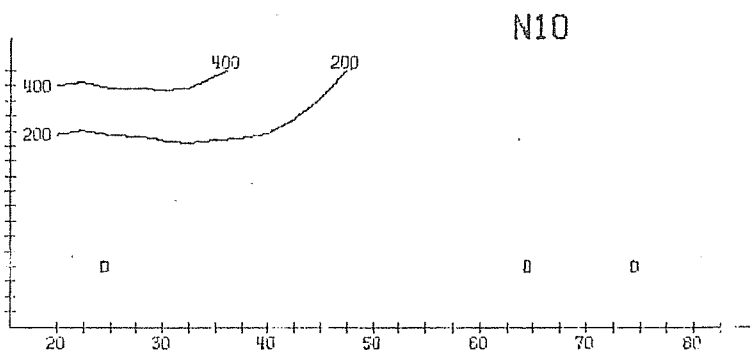
N10

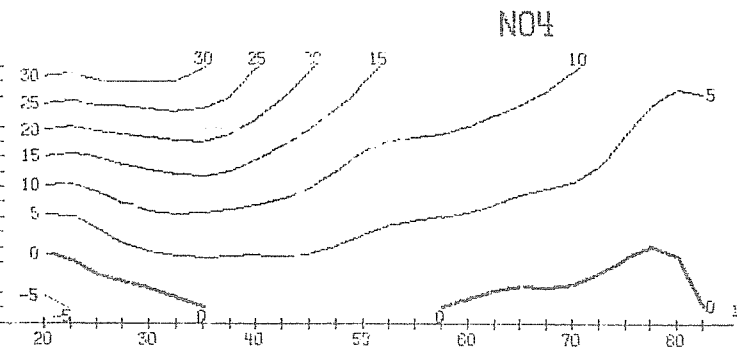
N04

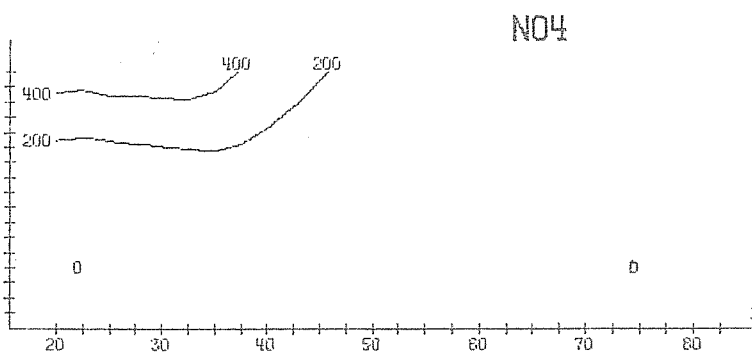
N04

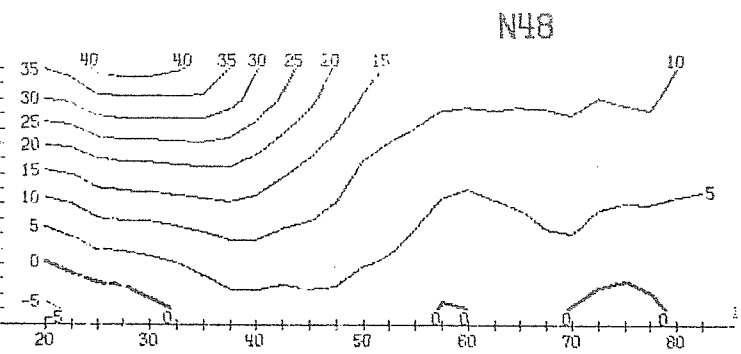
N48

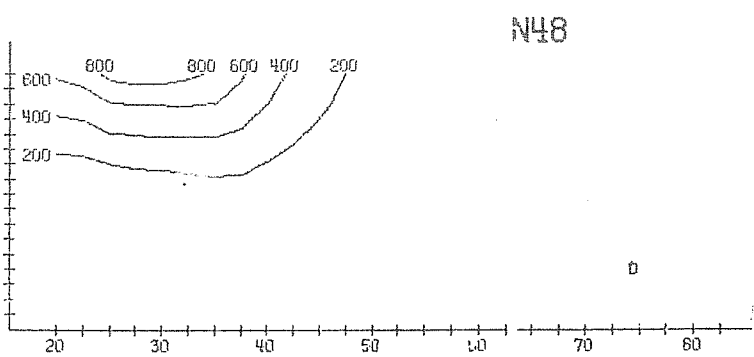
N48

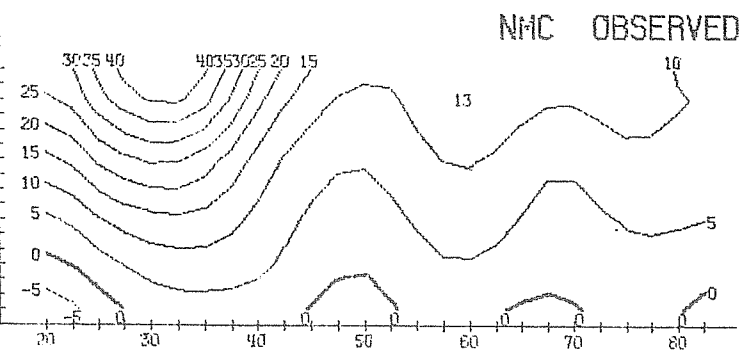
NMC OBSERVED
DAY 6.0 TO 10.0
ZONAL MEAN OF ZONAL WIND

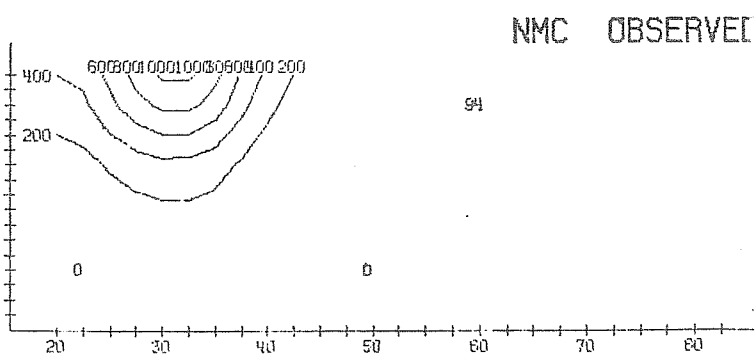
NMC OBSERVED
DAY 6.0 TO 10.0
ZONAL PART
KE (10 KJ/M2/BAR)

Figure 6

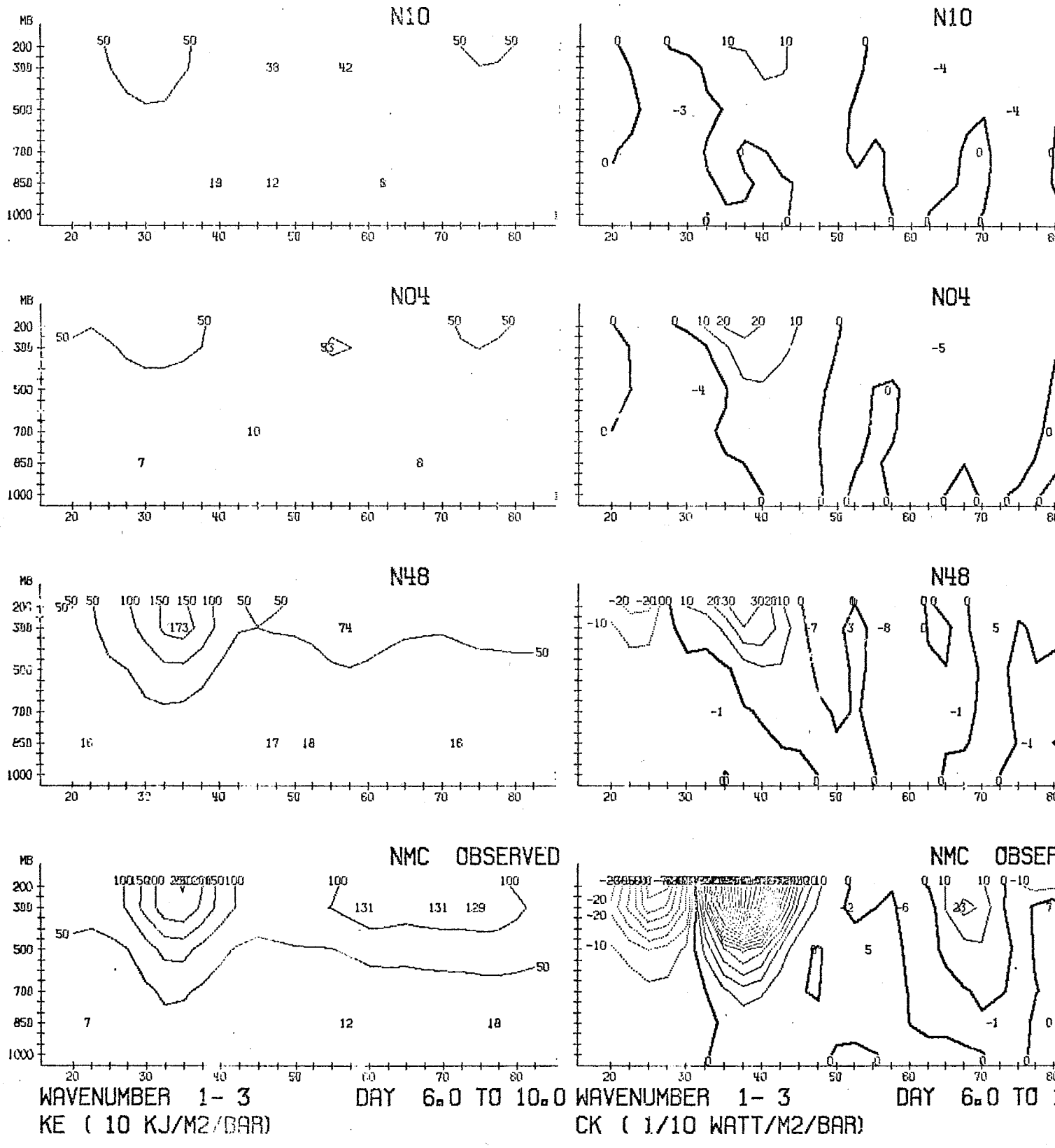

Figure 7 Latitude-height distribution of eddy kinetic energy KE and transformation of zonal kinetic energy into eddy kinetic energy for wavenumbers 1 - 3 .

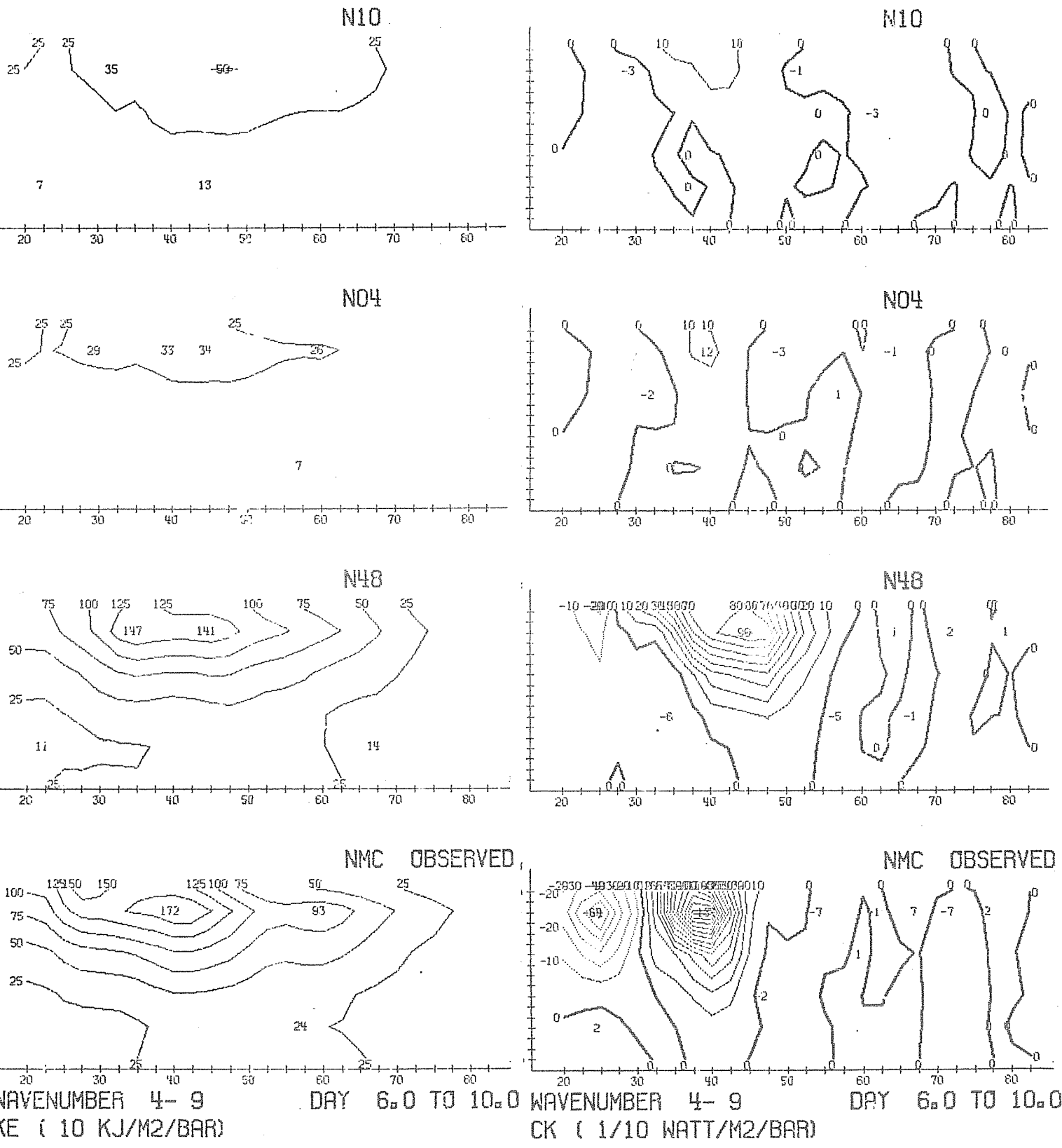

Figure 8 Latitude-height distribution of eddy kinetic energy KE and transformation of zonal kinetic energy into eddy kinetic energy for wavenumbers 4 to 9.

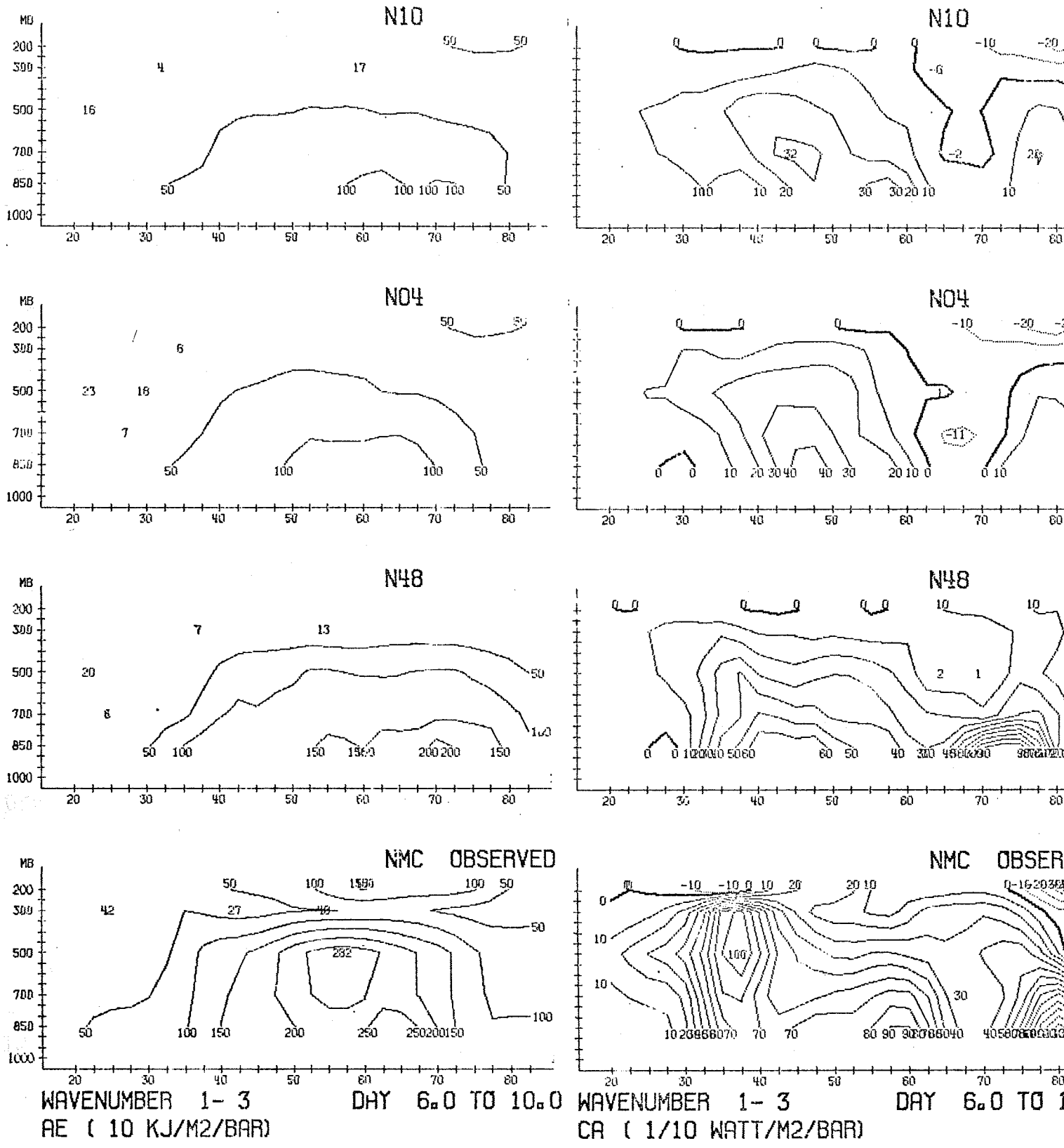

Figure 9 Latitude-height distribution of eddy available potential energy and transformation of zonal available potential energy into eddy available potential energy for wavenumb 1 to 3.

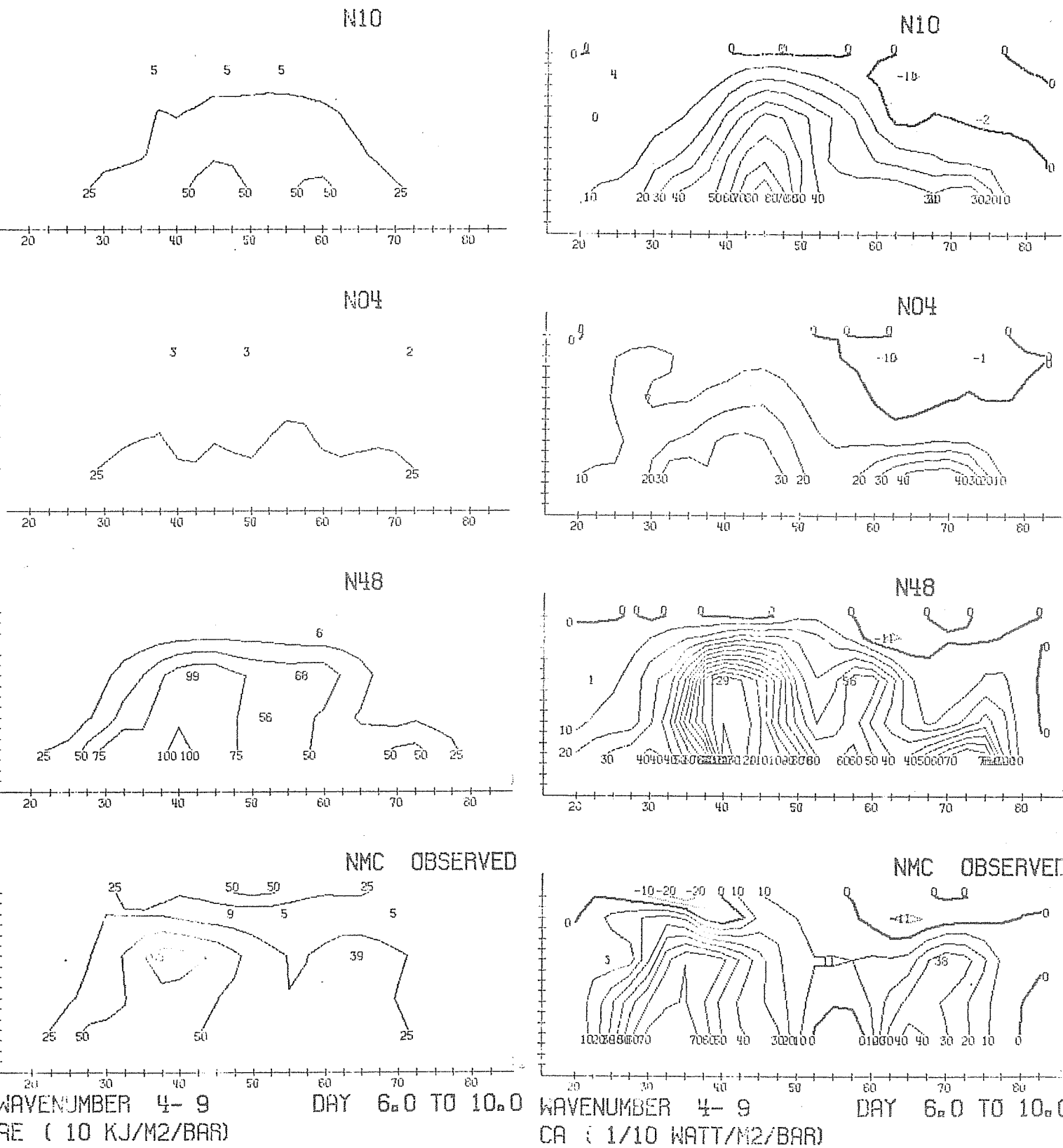

Figure 10 Latitude-height distributionof eddy available potential energy and transformation of zonal available potential energy into eddy available potential energy for wavenumbers 4 to 9.

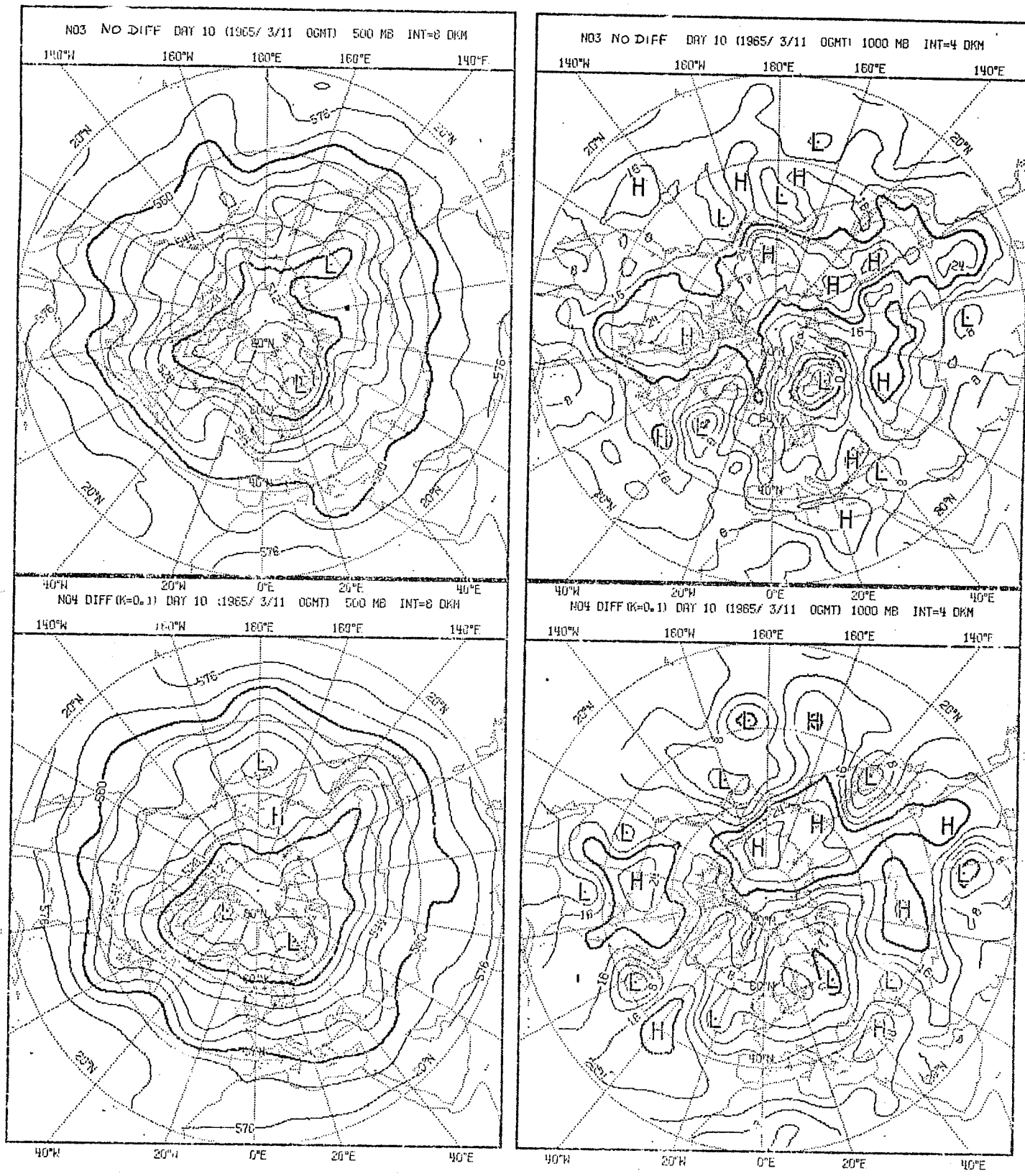

Figure 11 Distribution of height at 500 mb and at 1000 mb at day 10 (11.3.1965) for Run N03 and N04.

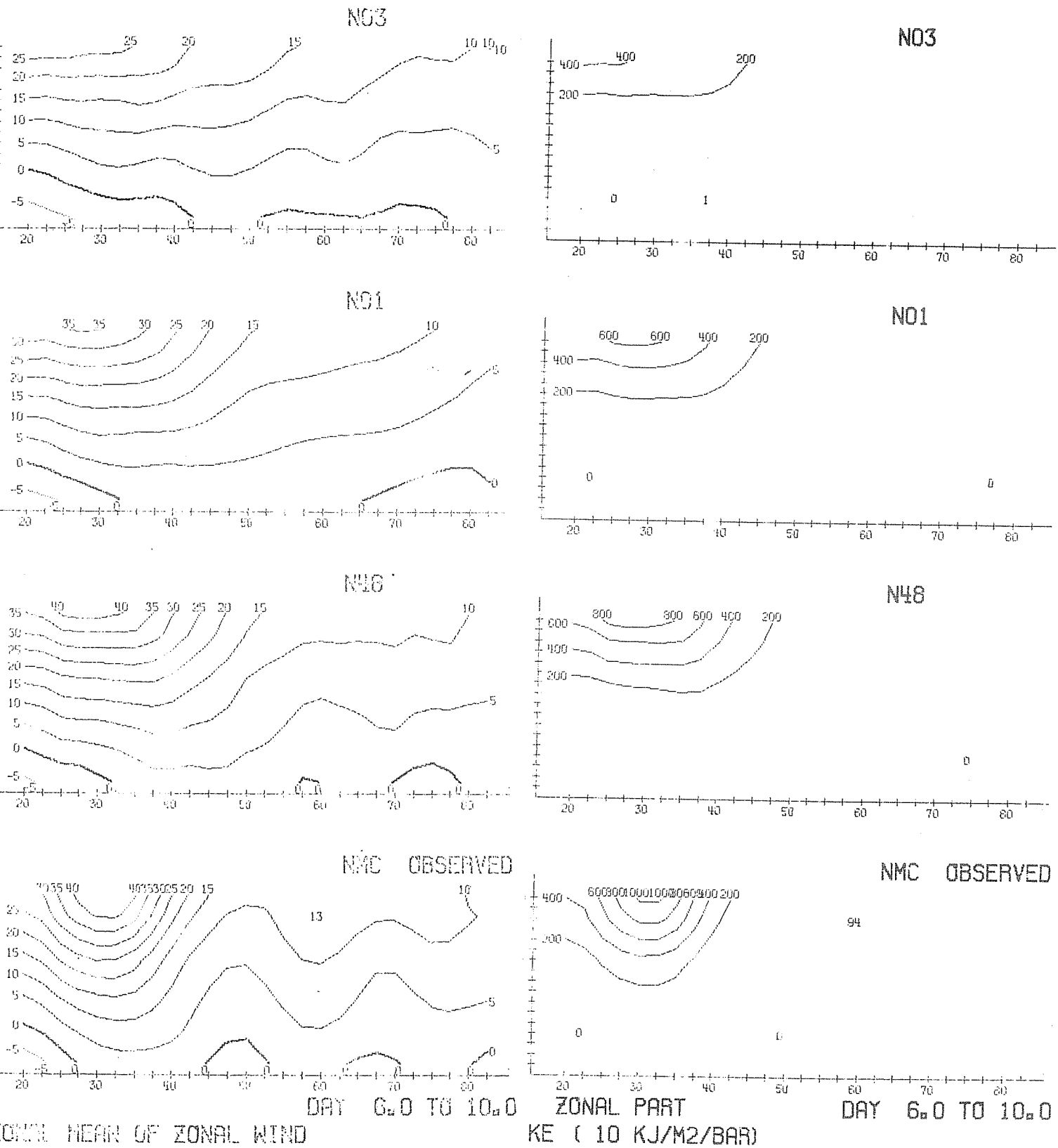
NO3
NO3
NO1
NO1
N48
N48
NMC OBSERVED
NMC OBSERVED
DAY 6.0 TO 10.0
ZONAL PART
DAY 6.0 TO 10.0
KE (10 KJ/M2/BAR)

Figure 12

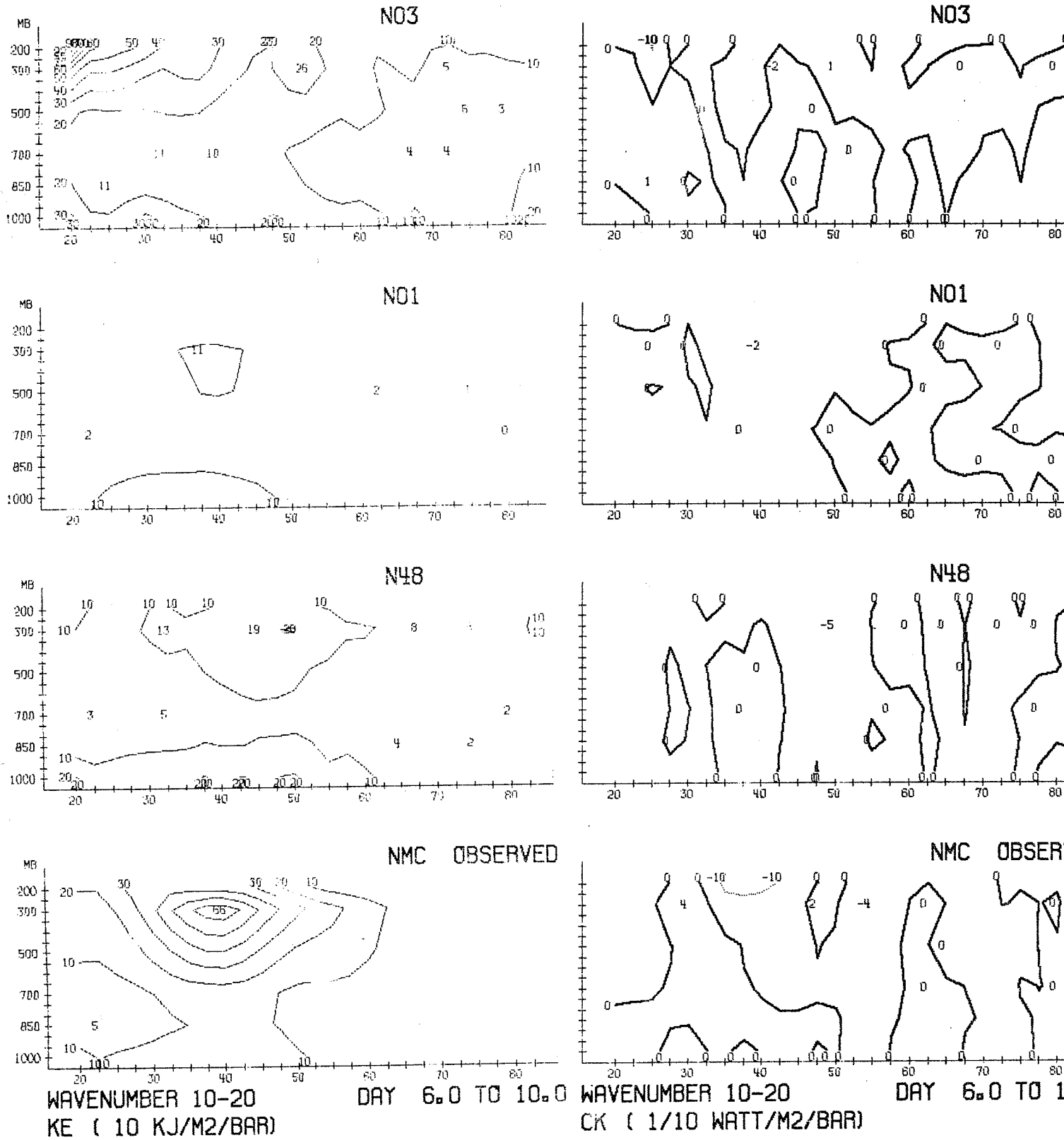

Figure 13 Latitude-height distribution of eddy kinetic energy KE and transformation of zonal kinetic energy into eddy kinetic energy for wavenumbers 10 to

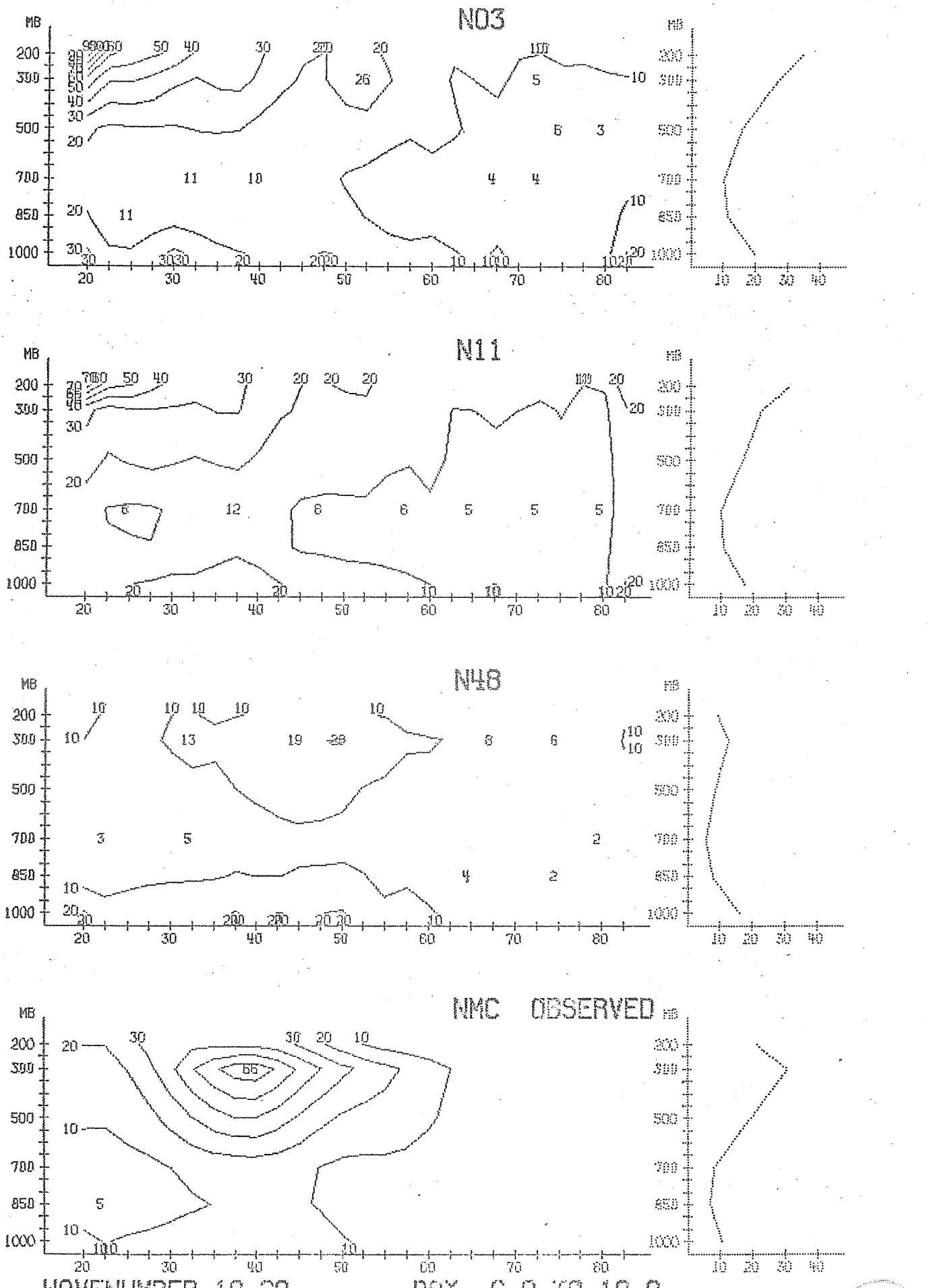

Figure 14 Latitude-height distributionof eddy kinetic energy for wavenumbers 10 to 20.

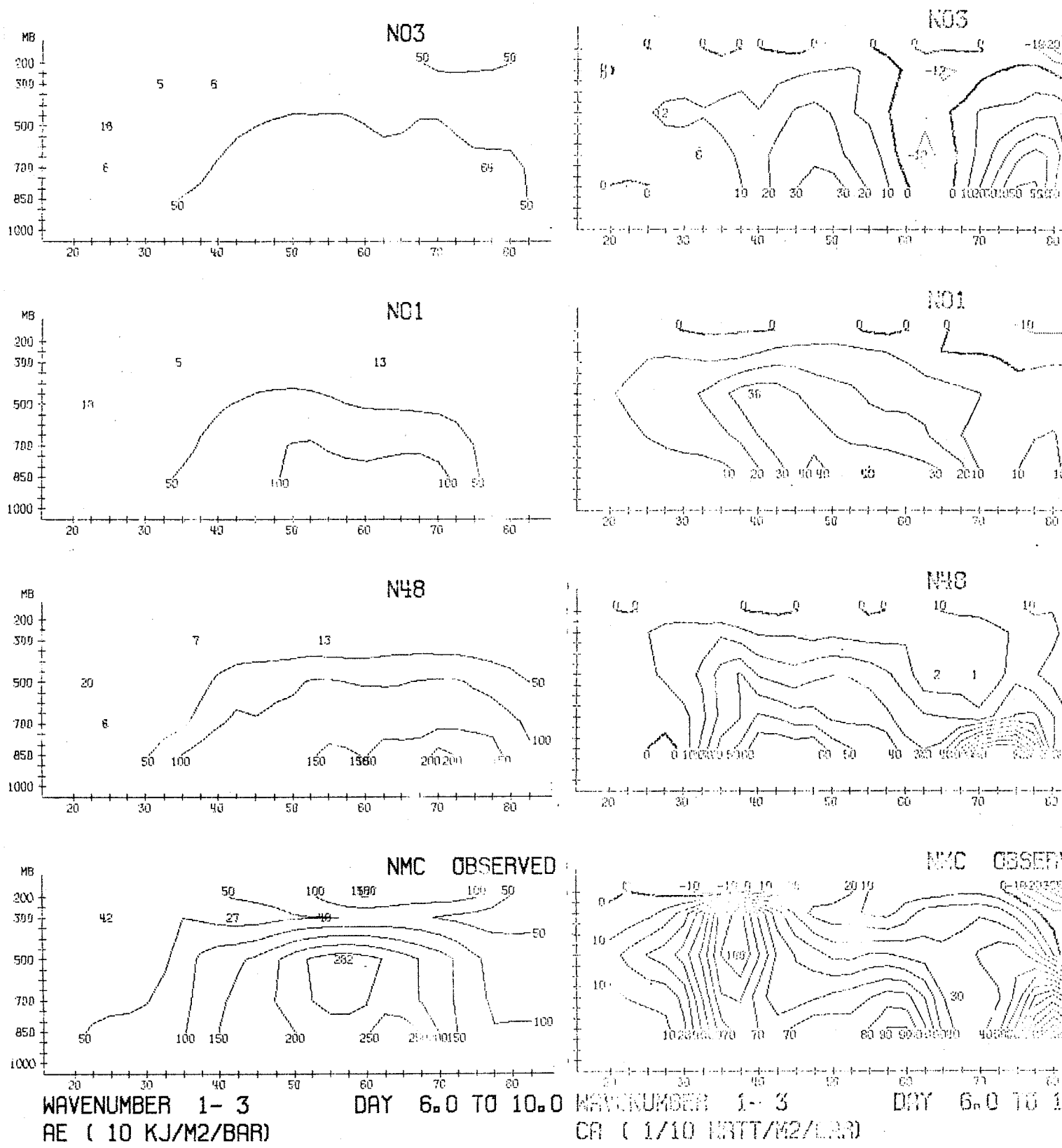

Figure 15 Latitude-height distribution of eddy available potential energy and transformation of zonal available potential energy into eddy available potential energy for wavenumbers 1 to 3.

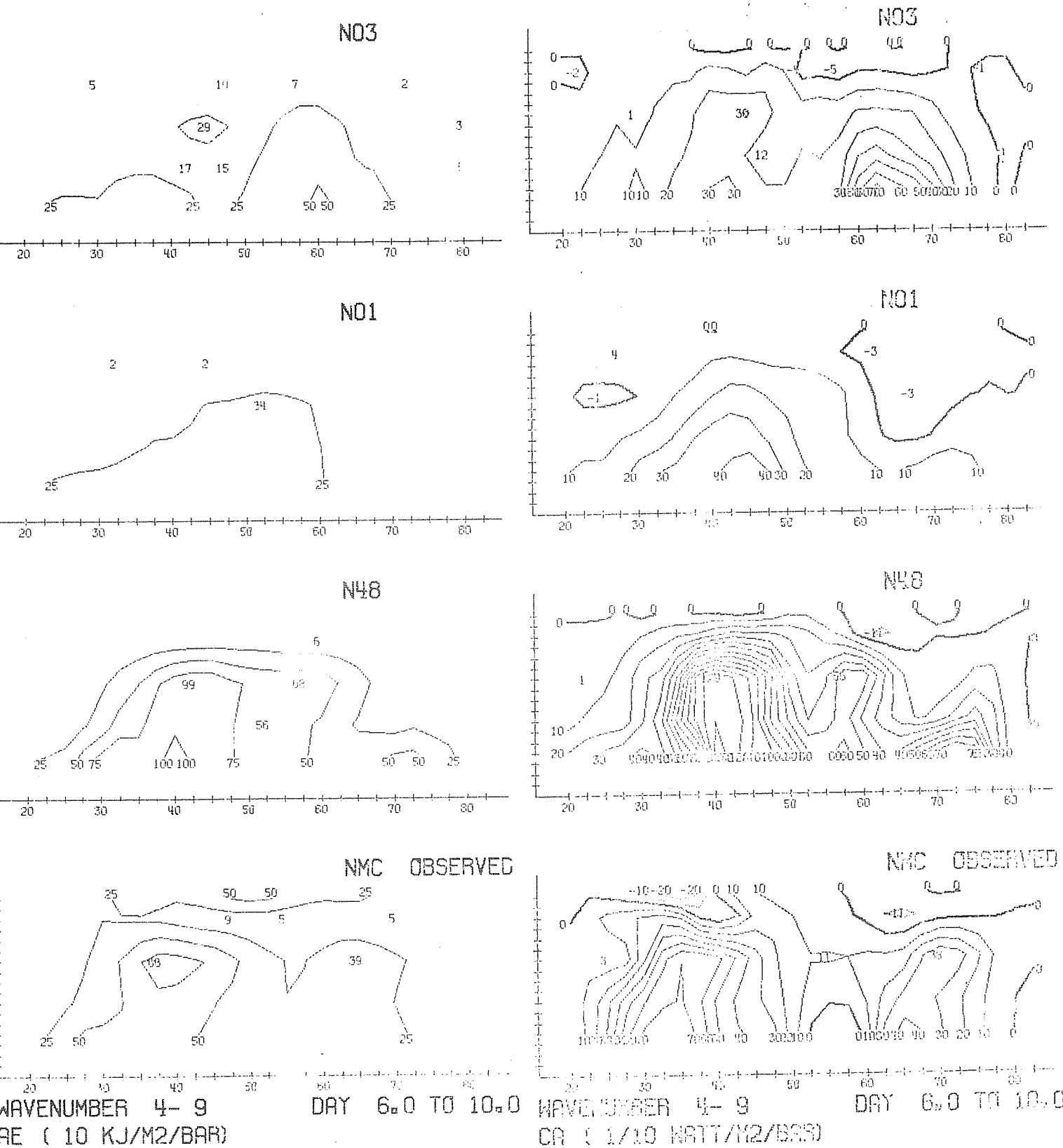

Figure 16 Latitude-height distribution of eddy available potential energy and transformation of zonal available potential energy into eddy available potential energy for wavenumbers 4 to 9.

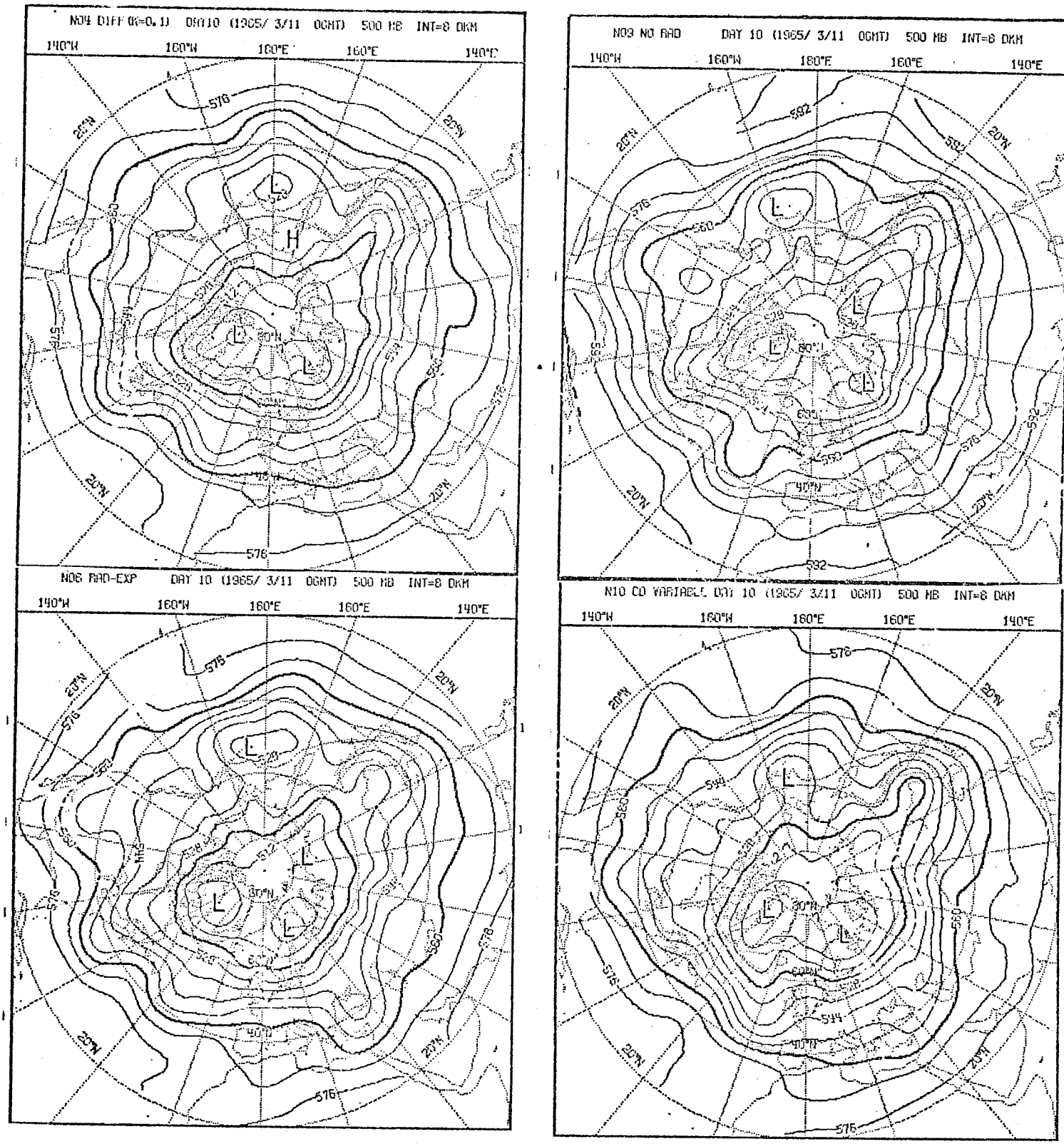

Figure 17 Height at 500 mb at day 10 (11.3.1965) for Run N04, N06, N09 and N10.

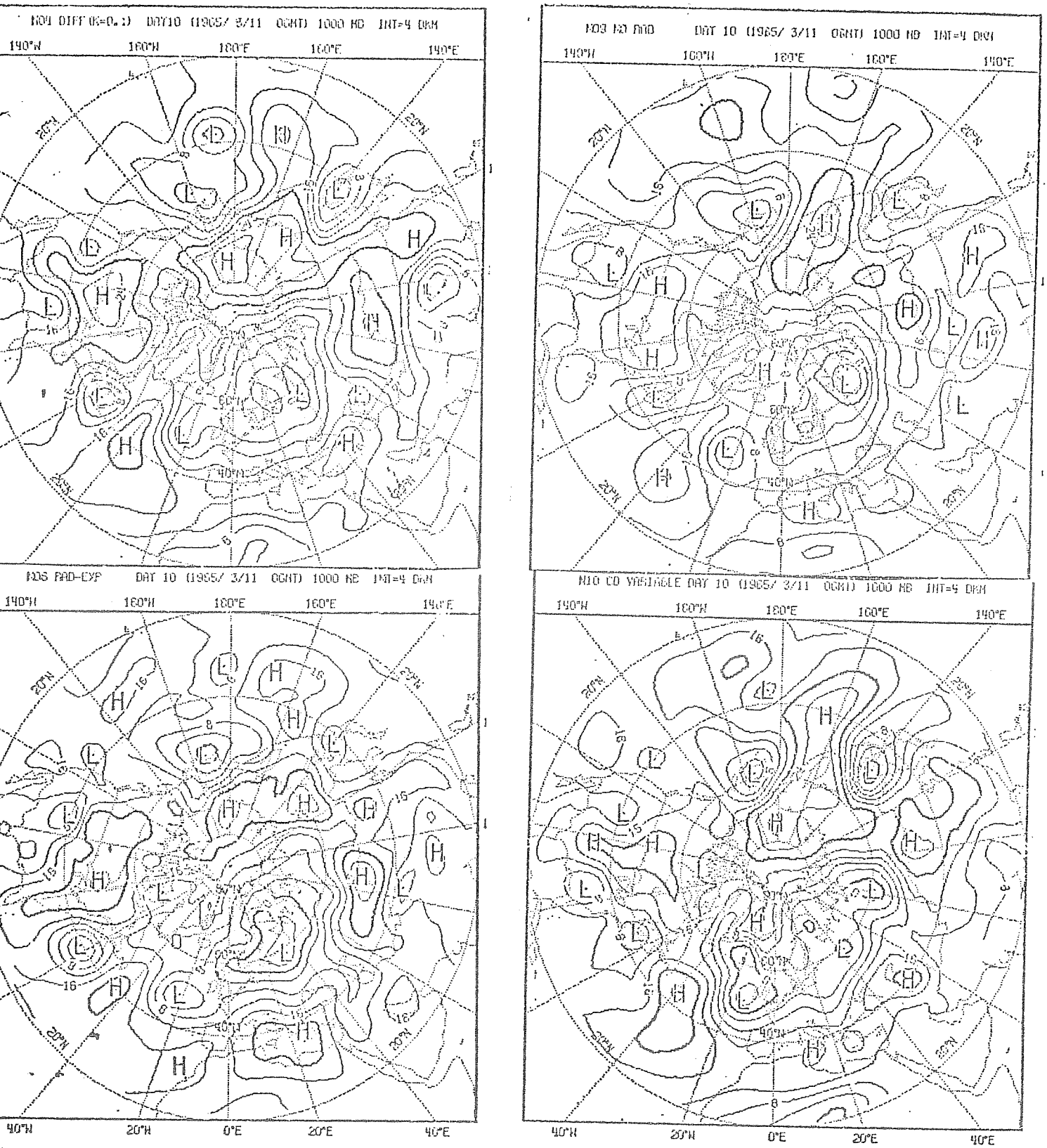

Figure 18 Height at 1000 mb at day 10 (11.3.1965) for Run N04, N06, N09, N10.

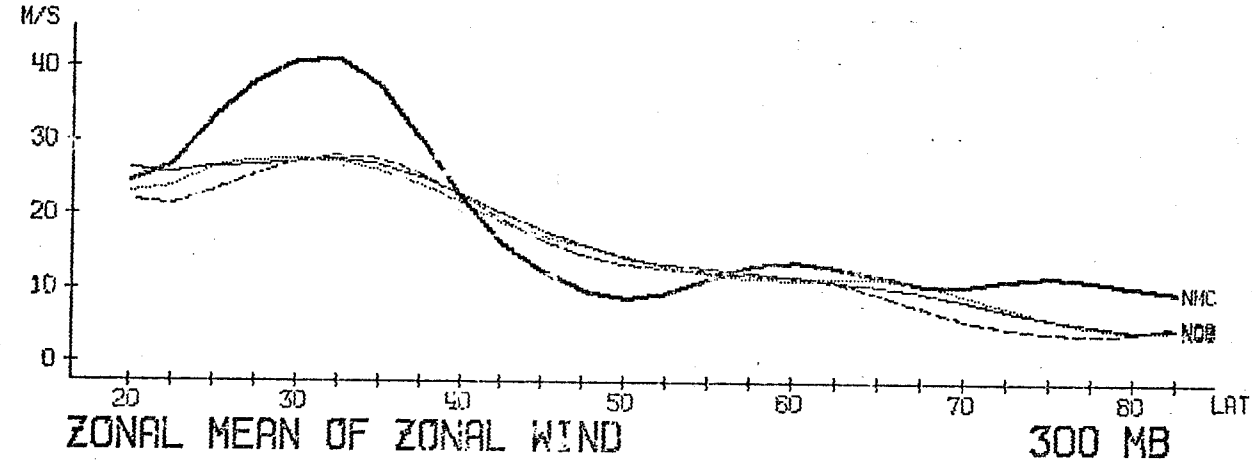
M/S
40
30
20
10
0
20
30
40
50
60
70
80
LAT
NMC
NO9
ZONAL MEAN OF ZONAL WIND
300 MB

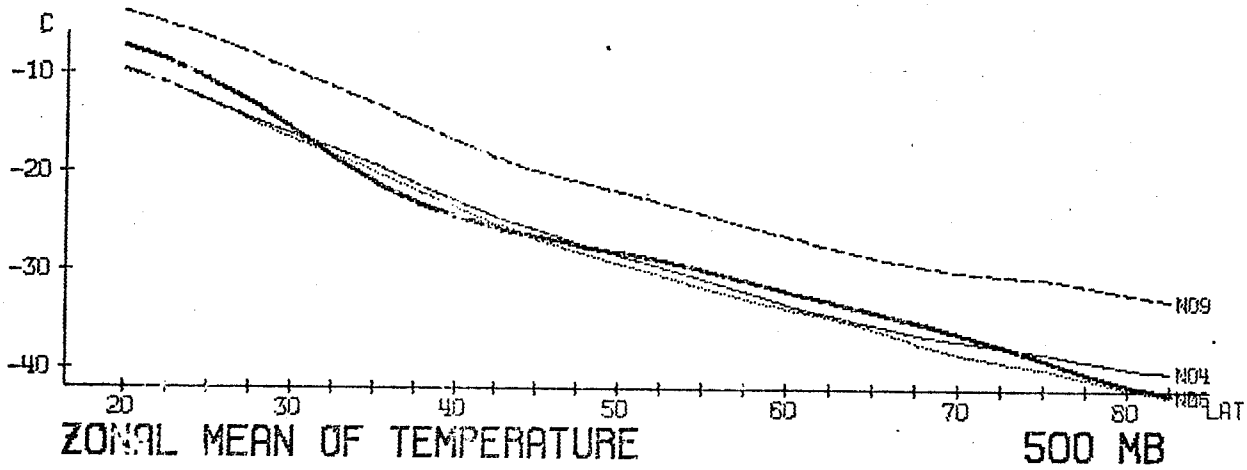
C
-10
-20
-30
-40
20
30
40
50
60
70
80
LAT
NO9
NO4
NO5
ZONAL MEAN OF TEMPERATURE
500 MB

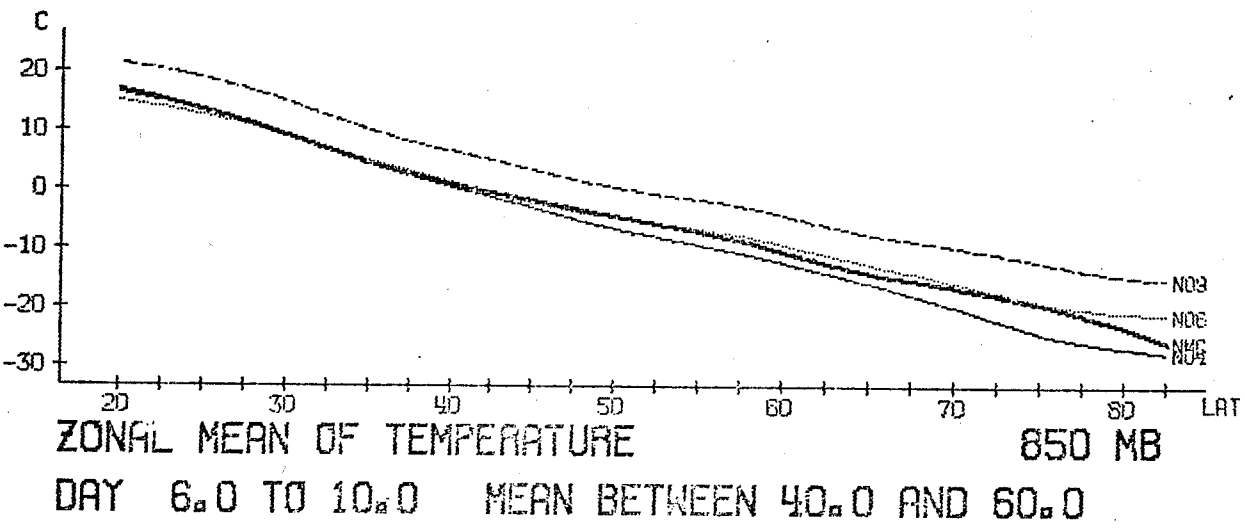
C
20
10
0
-10
-20
-30
20
30
40
50
60
70
80
LAT
NO9
NO6
NMC
NO4
ZONAL MEAN OF TEMPERATURE
850 MB
DAY 6.0 TO 10.0 MEAN BETWEEN 40.0 AND 60.0

Figure 19

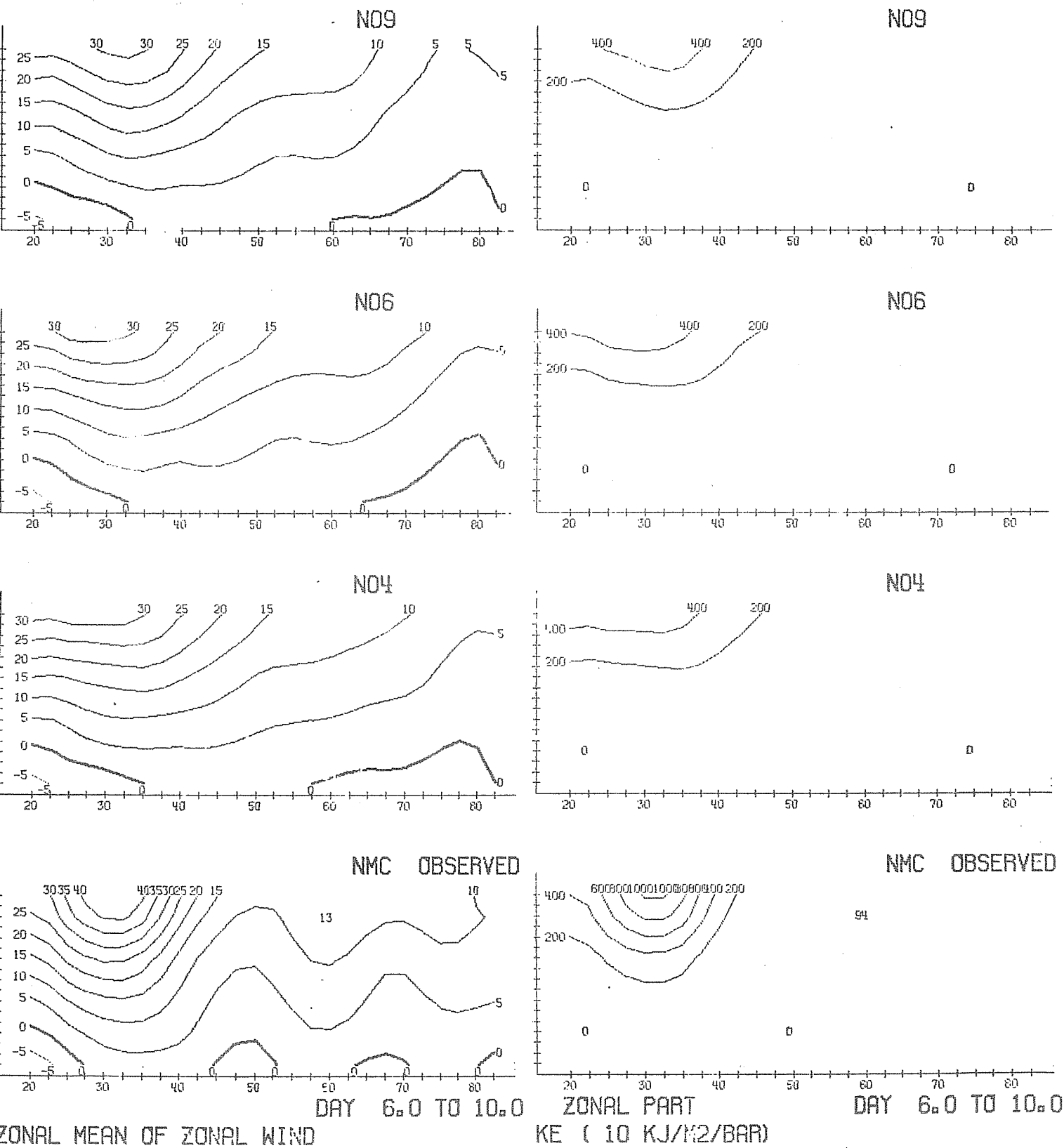
N09
N09
N06
N06
N04
N04
NMC OBSERVED
NMC OBSERVED
DAY 6.0 TO 10.0
ZONAL MEAN OF ZONAL WIND
ZONAL PART
DAY 6.0 TO 10.0
KE (10 KJ/M2/BAR)

Figure 20

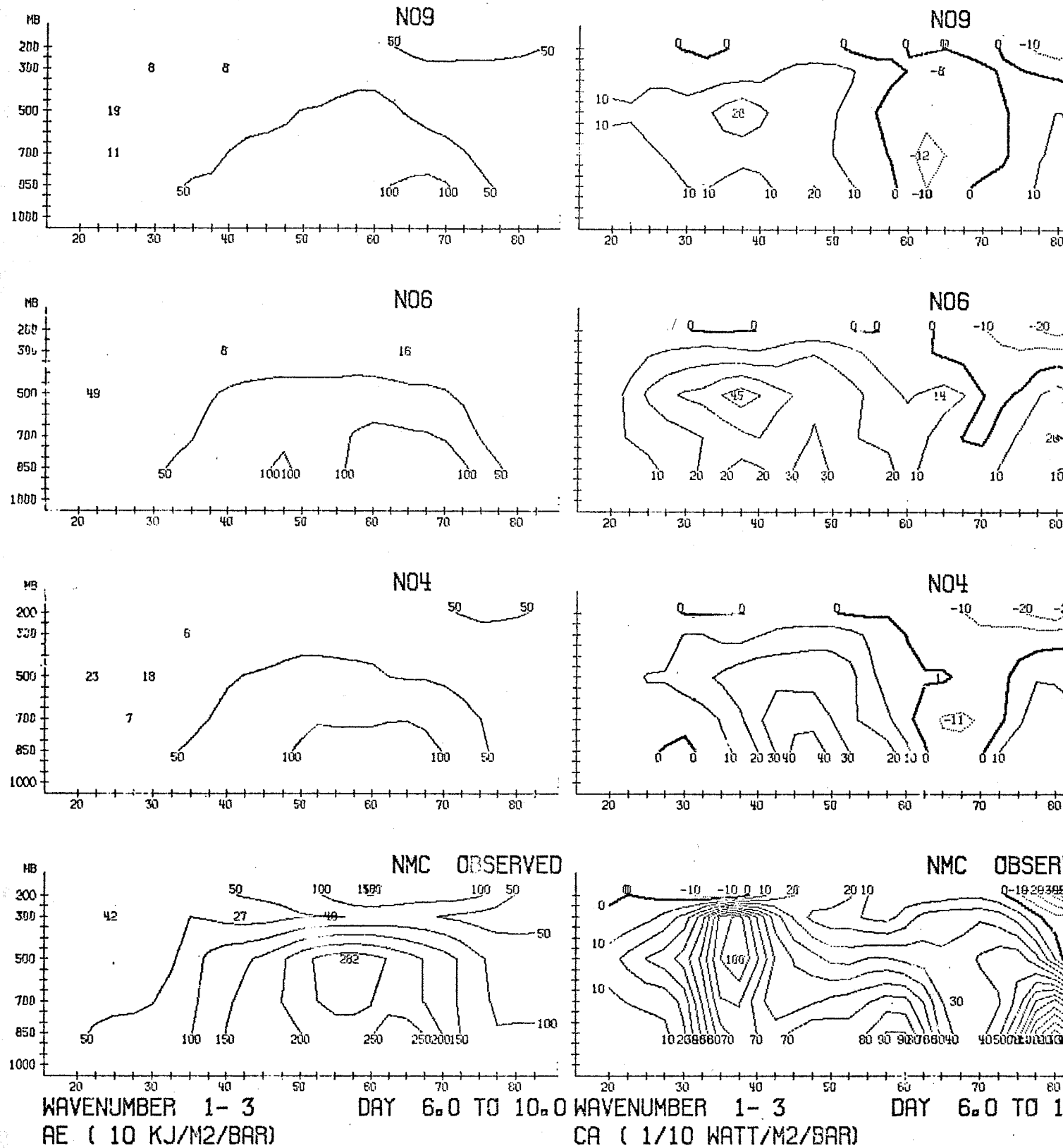

Figure 21 Latitude-height distribution of eddy available potential energy and transformation of zonal available potential energy into eddy available potential energy for wavenumbers 1 to 3.

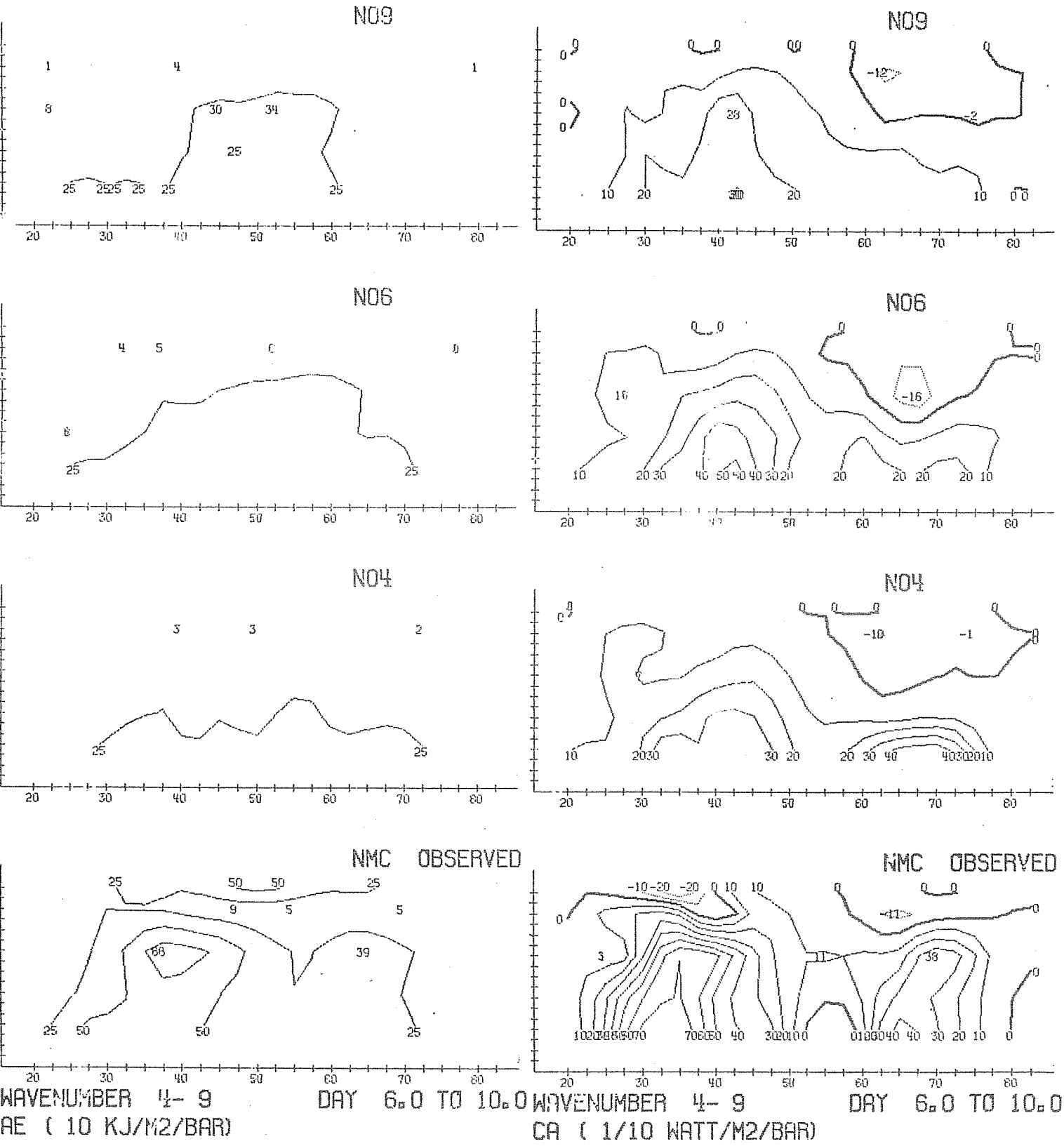

Figure 22 Latitude-height distribution of eddy available potential energy and transformation of zonal available potential energy into eddy available potential energy for wavenumbers 4 to 9.

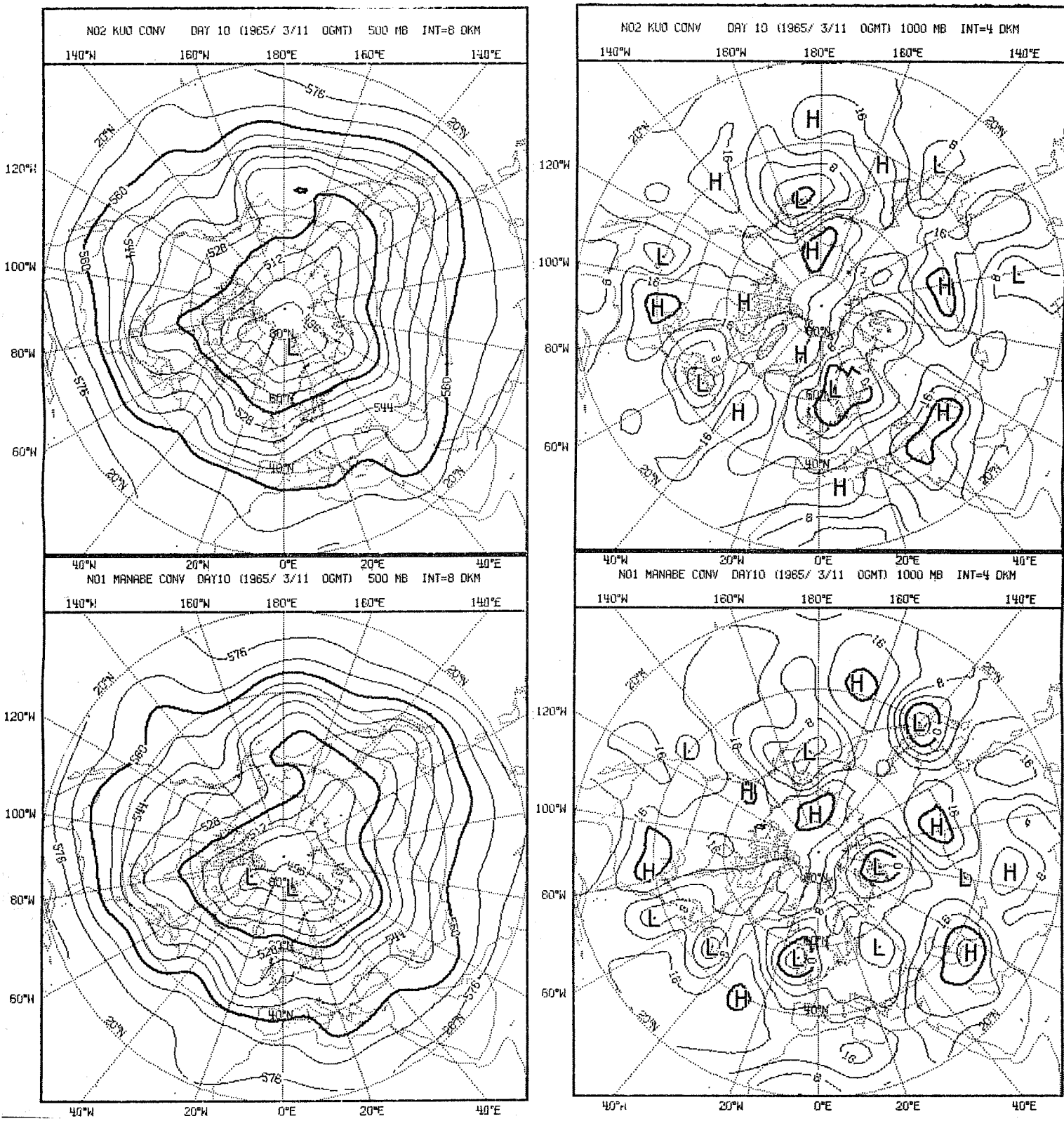

Figure 23 Distribution of height at 500 mb and 1000 mb at day 10 (11.3.1965) for Run N01 and N02.

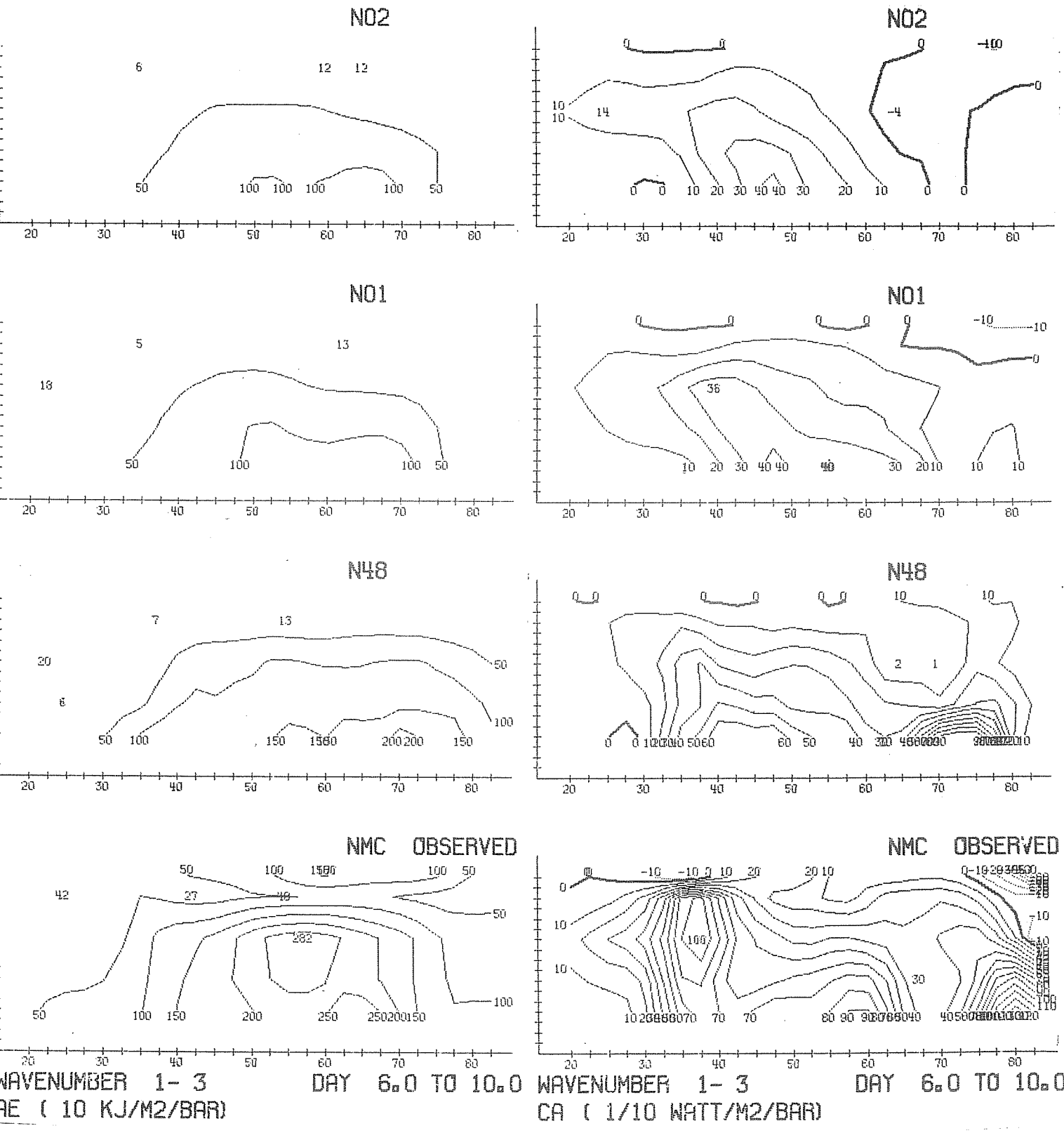

Figure 24 Latitude-height distribution of eddy available potential energy and transformation of zonal available potential energy into eddy available potential energy for wavenumbers 1 to 3.

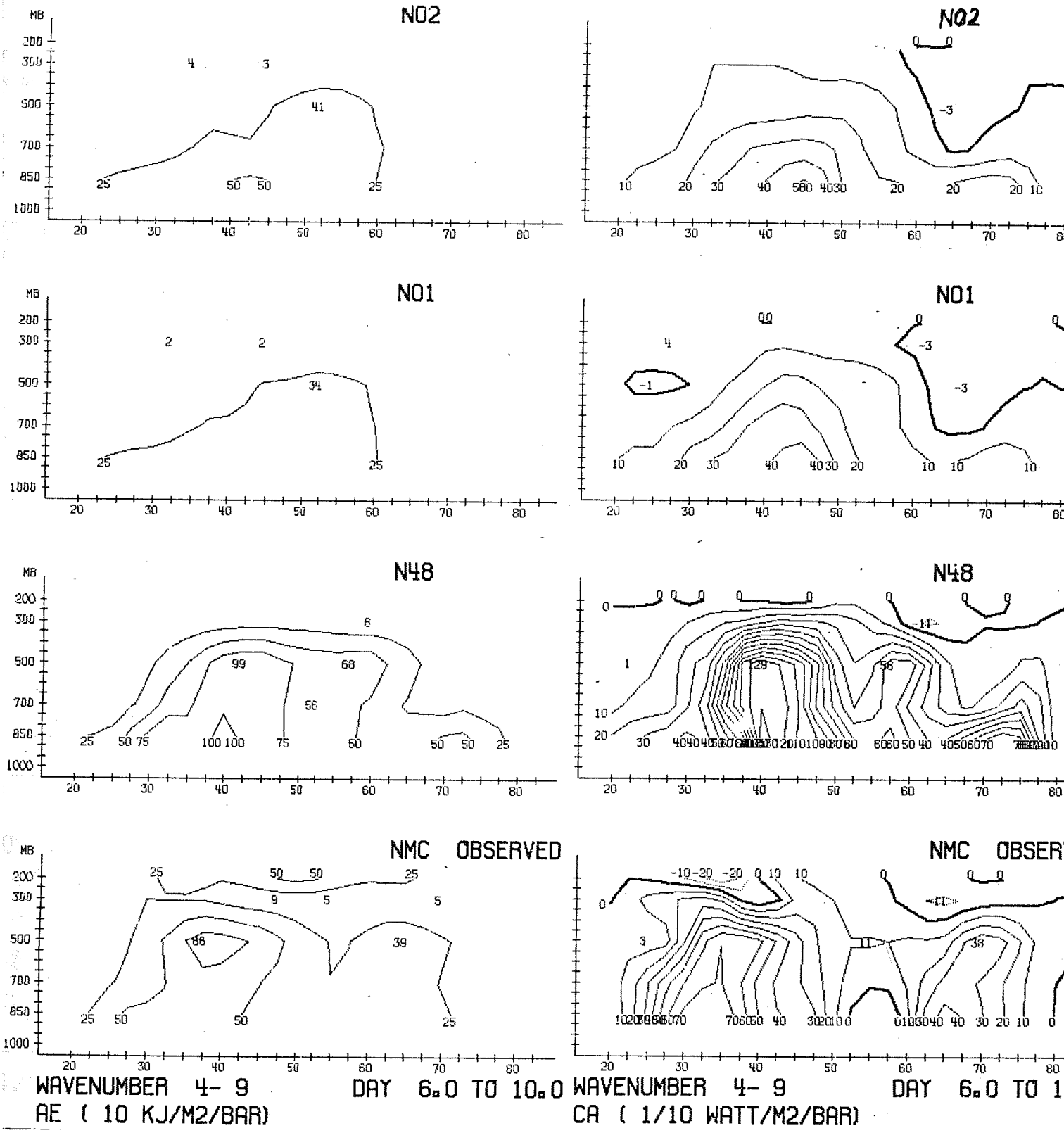

Figure 25 Latitude-height distribution of eddy available potential energy and transformation of zonal available potential energy into eddy available potential energy for wavenumbers 4 to 9.

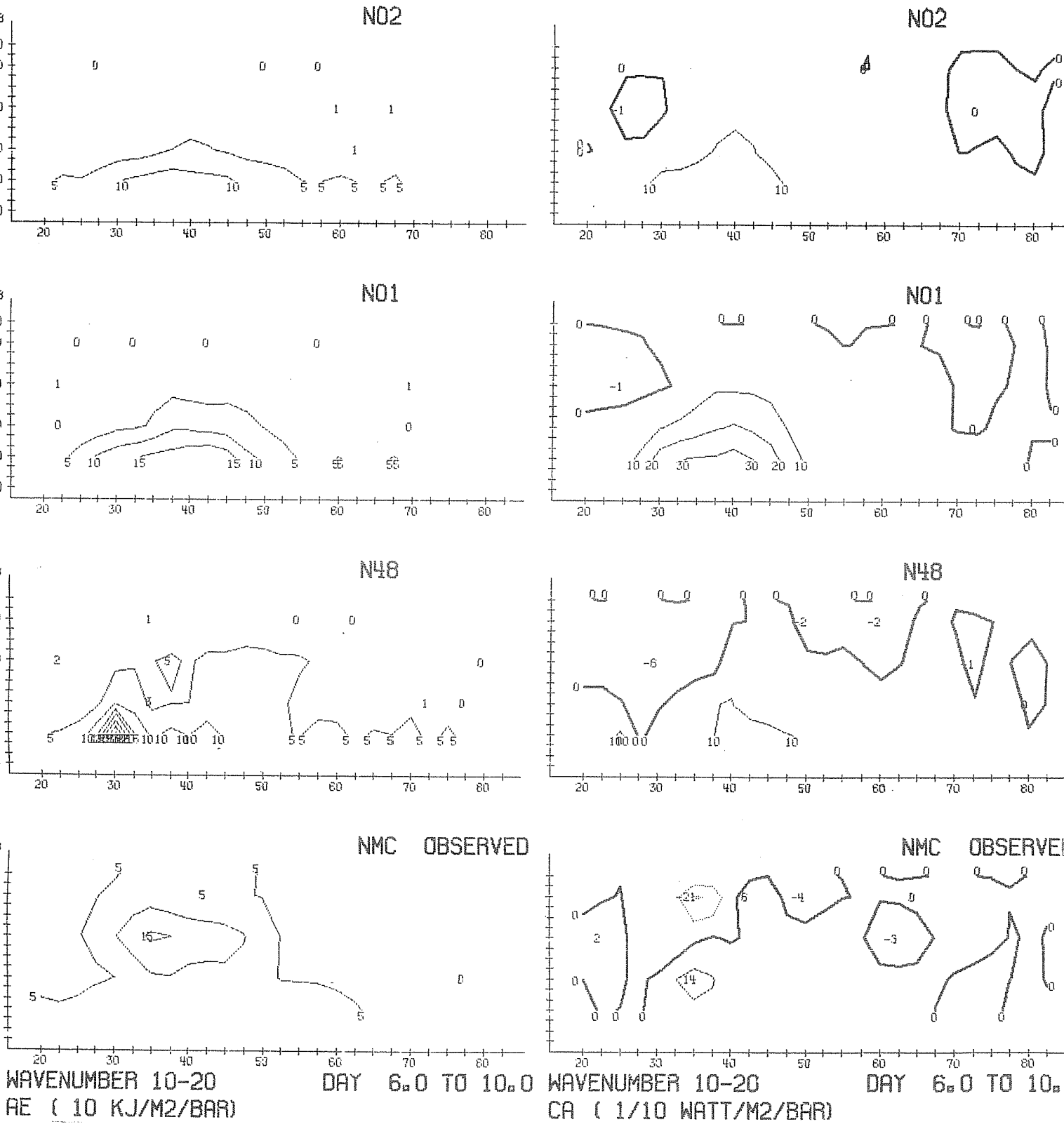

Figure 26 Latitude-height distribution of eddy available potential energy and transformation of zonal available potential energy into eddy available potential energy for wavenumbers 10 to 20.

References:

Anthes, R.A. (1977) A cumulus parameterization scheme utilising a one-dimensional cloud model. Mon.Wea.Rev.,105, pp.270-286.

Budyko,M.I. (1956) Heat balance of the earth's surface. Leningrad. 225 pp.

Burridge, D.M. and J. Haseler (1977) A model for medium-range weather forecasting - Adiabatic Formulation. ECMWF Technical Report No. 4.

Deardorff, J.W. (1971) On the magnitude of the subgrid scale eddy coefficient. Journal of Comp.Phys.7, pp. 120 - 133.

Geleyn, J.-F. (1977) A comprehensive radiation scheme designed for fast computation. ECMWF Internal Report No. 8.

Kessler, E. (1969) On the distribution and continuity of water substance in atmospheric circulations. Met.Monogr. Amer.Met.Soc. 10, 84 pp.

Kuo, H.L. (1965) On formation and intensification of tropical cyclones through latent heat release by cumulus convection. J.Atmos.Sci. 22, pp. 40 - 63.

Kuo, H.L. (1974) Further studies of the parameterization of the influence of cumulus convection on large-scale flow. J.Atmos.Sci.,31, pp. 1232-1240.

Louis, J.-F. (1977) Parameterization of the surface fluxes. ECMWF Internal Report No. 4.

Manabe, S. Smagorinsky,J. and Strickler,R.F. (1965) Simulated climatology of a general circulation model with a hydrologic cycle. Mon.Wea.Rev.93, pp.769-798.

References:

Miyakoda, K. et al (1971) "The effect of horizontal grid resolution in an atmospheric circulation model". J. Atmos. Sci., 28, pp.481-499.

Miyakoda, K. (1975) "Weather forecasts and the effects of the subgrid scale processes". Notes on ECMWF Seminars 1-12.9.75. pp. 380 - 595.

Smagorinsky, J. (1963) "General circulation experiments with the primitive equations". 1. The basic experiment . Mon. Wea. Rev. 91, pp. 99-164.

Temperton, C. (1977) "Normal modes of a barotropic version of the ECMWF gridpoint model". ECMWF, Internal Report No. 12.